

#### **OPEN ACCESS**

EDITED BY Vivek Venkataraman, University of Calgary, Canada

REVIEWED BY
André Pinheiro,
Rio de Janeiro State University, Brazil
Davide Tamagnini,
Sapienza University of Rome, Italy

\*CORRESPONDENCE
Laurent Pallas

☑ laurent.pallas01@univ-poitiers.fr

RECEIVED 14 March 2025 ACCEPTED 03 September 2025 PUBLISHED 16 October 2025

#### CITATION

Pallas L, Nakatsukasa M, Daver G, Guy F, Rio N and Rowan J (2025) New femoral evidence from the Afar reveal the early evolution of habitual squatting behaviors in the genus *Theropithecus*. *Front. Ecol. Evol.* 13:1593646. doi: 10.3389/fevo.2025.1593646

#### COPYRIGHT

© 2025 Pallas, Nakatsukasa, Daver, Guy, Rio and Rowan. This is an open-access article distributed under the terms of the Creative Commons Attribution License (CC BY). The use, distribution or reproduction in other forums is permitted, provided the original author(s) and the copyright owner(s) are credited and that the original publication in this journal is cited, in accordance with accepted academic practice. No use, distribution or reproduction is permitted which does not comply with these terms.

# New femoral evidence from the Afar reveal the early evolution of habitual squatting behaviors in the genus *Theropithecus*

Laurent Pallas<sup>1,2,3\*</sup>, Masato Nakatsukasa<sup>1</sup>, Guillaume Daver<sup>2</sup>, Franck Guy<sup>2</sup>, Noam Rio<sup>2</sup> and John Rowan<sup>4</sup>

<sup>1</sup>Graduate School of Science, Laboratory of Physical Anthropology, Kyoto University, Kyoto, Japan, <sup>2</sup>Laboratoire de Paléontologie, Évolution, Paléoécosystèmes et Paléoprimatologie (PALEVOPRIM), UMR 7262, Université de Poitiers, Poitiers, France, <sup>3</sup>UMR 7194, CNRS, Département Homme & Environnement, Muséum National D'Histoire Naturelle, Musée de L'Homme, Paris, France, <sup>4</sup>Department of Archaeology, University of Cambridge, Cambridge, United Kingdom

**Introduction:** The femoral anatomy of fossil *Theropithecus* is poorly known, although it provides critical data for inferring squatting behaviors, a characteristic trait of extant *Theropithecus gelada*.

**Methods:** Here, we describe and provide functional and taxonomic interpretations on two subcomplete femora from the Afar Depression using a combination of traditional morphometrics (bivariate and multivariate) and 2D geometric morphometric combined with multivariate analyses and hierarchical clustering.

**Results:** The ca. 3.20 Ma A.L. 206–1 femur is identified as the oldest known and most complete femur of an adult *Theropithecus* cf. oswaldi darti and shows a morphology similar to that of extant *T. gelada*. It supports the hypothesis of an early emergence of squatting behaviors in *Theropithecus*, prior to the onset of dental adaptations related to the grazing diet of the genus. The ca. 2.60 Ma A.L. 94–5 femur is identified as the oldest and most complete femur known of an adult *Theropithecus* cf. oswaldi oswaldi. Its knee anatomy is distinct from that of *T. o. darti* but it nonetheless shares with *T. gelada* and other fossil *Theropithecus* functional traits related to squatting behaviors. Unexpected convergences with arboreal cercopithecids are observed in *Theropithecus brumpti*, indicating diversity in the femoral functional anatomy of *Theropithecus*.

**Discussion:** Overall, our study highlights the future need to link femoral anatomical diversity with postural and locomotor behaviors by combining paleontological data with neontological data including biomechanical data on the squatting and climbing of large extant papionins.

KEYWORDS

Hadar, plio pleistocene, functional anatomy, evolutionary biology, Cercopithecidae

#### Introduction

From the early 1970s onwards, the discovery of hundreds of hominin fossils (Johanson et al., 1982a; White and Johanson, 1982; Susman et al., 1984; Latimer et al., 1987; Kimbel et al., 1994; Drapeau et al., 2005; Kimbel and Delezene, 2009; Ward et al., 2012; DeSilva et al., 2020) in 3.40-2.95 Ma fluviolacustrine sediments from the Hadar Formation has shed light on the paleobiodiversity of fossiliferous localities from the Hadar Research Project area (Bonnefille et al., 1987; Radosevich et al., 1992; Behrensmeyer, 2008; Reed, 2008; Campisano et al., 2022), in the Afar Depression, Ethiopia (Figure 1). The search for hominin remains also vielded detailed chronostratigraphic frameworks and an extensive mammalian fossil record (Johanson et al., 1982b; Campisano and Feibel, 2007, 2008). Similarly, a large mammalian fossil record has been discovered alongside the earliest Homo specimens in the younger deposits of nearby Ledi-Geraru (Lee Adoyta basin, ca. 2.8 Ma) and the Busidima Formation at Hadar (ca. 2.35-2 Ma) (Kimbel et al., 1996; Campisano, 2012; Villmoare et al., 2015; Rowan et al., 2022). Fossil cercopithecids figure prominently in the fossil record of the oldest deposits of the Hadar Formation, with well-preserved isolated craniodental and postcranial specimens recovered alongside three partial skeletons, including the holotype of the fossil colobine Cercopithecoides meavae and the sole partial skeleton of Parapapio jonesi (Eck, 1993; Krentz, 1993; Frost and Delson, 2002; Rector and Vergamini, 2018). There is evidence of cercopithecid taxonomic diversity at Hadar with the presence of the large colobine Rhinocolobus turkanaensis and the medium-sized papionin Parapapio jonesi, but most cercopithecid fossil specimens were attributed to Theropithecus oswaldi darti, one of the earliest Theropithecus (Frost and Delson, 2002). Specimens of cercopithecids from outcrops of the Busidima Formation at Hadar and the Lee Adoyta basin at Ledi-Geraru have not been formally described, but T. o. darti was provisionally recorded at Lee Adoyta and Gurumaha fault blocks at Ledi-Geraru (DiMaggio et al., 2015).

The taxonomy of early *Theropithecus* is in flux, as illustrated by the recent naming of Theropithecus oswaldi ecki, which recognizes the phyletic distinctiveness of the early eastern African Theropithecus compared from T. o. darti of the southern African site of Makapansgat (Getahun et al., 2023). This led Getahun et al. (2023) to transfer specimens from Hadar, as well as those from Dikika, to T. o. ecki. The distinct subspecies status of T. o. ecki was largely established on its smaller dental size compared with southern African specimens of T. o. darti along with qualitative mandibular and cranial features, but not postcranial traits, despite the inclusion of postcranial specimens in paratypes of T. o. ecki. Furthermore, only the fragmentary proximal femora A.L. 175-2 and A.L. 341-5a were formally published and tentatively assigned to T. o. darti (Delson et al., 1993; Krentz, 1993; Frost and Delson, 2002). Recent advances in our knowledge of the postcranial anatomy of early Theropithecus were achieved by the description of the ca. 3.60 Ma Theropithecus subadult partial skeleton ARI-VP-

1/26 from Woranso-Mille, attributed to T. o. darti (Frost et al., 2023). ARI-VP-1/26 demonstrated, among other characteristics, that the metacarpal proportions typical of Theropithecus (i.e., elongated first metacarpal relative to the average lengths of all other metacarpals) were not yet present in early Theropithecus, with proportions intermediate between those of extant Papio and Theropithecus gelada (Frost et al., 2023). No clear assessment of traits related to squatting behaviors, such as the anteroposterior asymmetry of the femoral condyles, was done on ARI-VP-1/26. Frost et al. (2023) nonetheless noted the presence of a short femur and a varus knee in ARI-VP-1/26, the first trait functionally attributable to squatting while the functional value of the latter is unclear (Pallas et al., 2023). Novel hypotheses on the functional anatomy of the Theropithecus hindlimb were established thanks to the description of the associated femur and tibia of T. cf. brumpti NME L 896-1 and -2 (Shungura Formation, Lower Omo Valley, Ethiopia; Pallas et al., 2023). The associated morphofunctional analysis demonstrated that the angulation of the knee was variable and do not allow to distinguish T. gelada from other extant papionins. This is in contrast with the shortened femur, asymmetrical anteroposterior length of the femoral condyles, wide patellar groove, wide intercondylar notch, wide distal epiphysis and high crural index which distinguish T. gelada from other papionins (Gilbert et al., 2011; Pallas et al., 2023). This combination of characteristics was ultimately linked to the squatting and shuffling behaviors of T. gelada, which, in addition to altered craniodental anatomy and manual proportions, is linked to a grazing diet and careful handling of grass blades, respectively (Iwamoto, 1993). However, the assessment of the above combination of femoral characteristics is unknown in fossil Theropithecus predating 2.70 Ma due to the lack of complete femoral specimens. The discovery of two subcomplete femora (A.L. 94-5 and A.L. 206-1) from the Afar Depression, contemporaneous with, and predating this period, may shed light on the timing and context of the emergence of these postcranial femoral traits (Figure 1).

Here, we describe two subcomplete cercopithecid femora from the Hadar and Busidima formations. Using comparative anatomy and 2D geometric morphometrics, we provide functional hypotheses related to locomotor behaviors, in addition to providing taxonomic hypotheses. Specifically, we assess whether the subcomplete femora A.L. 94-5 and A.L. 206-1 can be attributed to Theropithecus and whether they exhibit traits related to the squatting behavior typical of T. gelada and later species of that genus. We confirm the attribution of these specimens to Theropithecus, with A.L. 206-1 being the oldest adult Theropithecus femur yet known and predating the previous evidence by around 500 kyr. A.L. 94-5 shows a greater phenetic affinity with presumed Theropithecus oswaldi oswaldi specimens and represent the oldest and most complete femur of this taxon. Our functional analyses of A.L. 206-1 and A.L. 94-5 has implications on the functional anatomy and evolution of Theropithecus, notably on the emergence of postural traits related to the grazing habits of that genus.

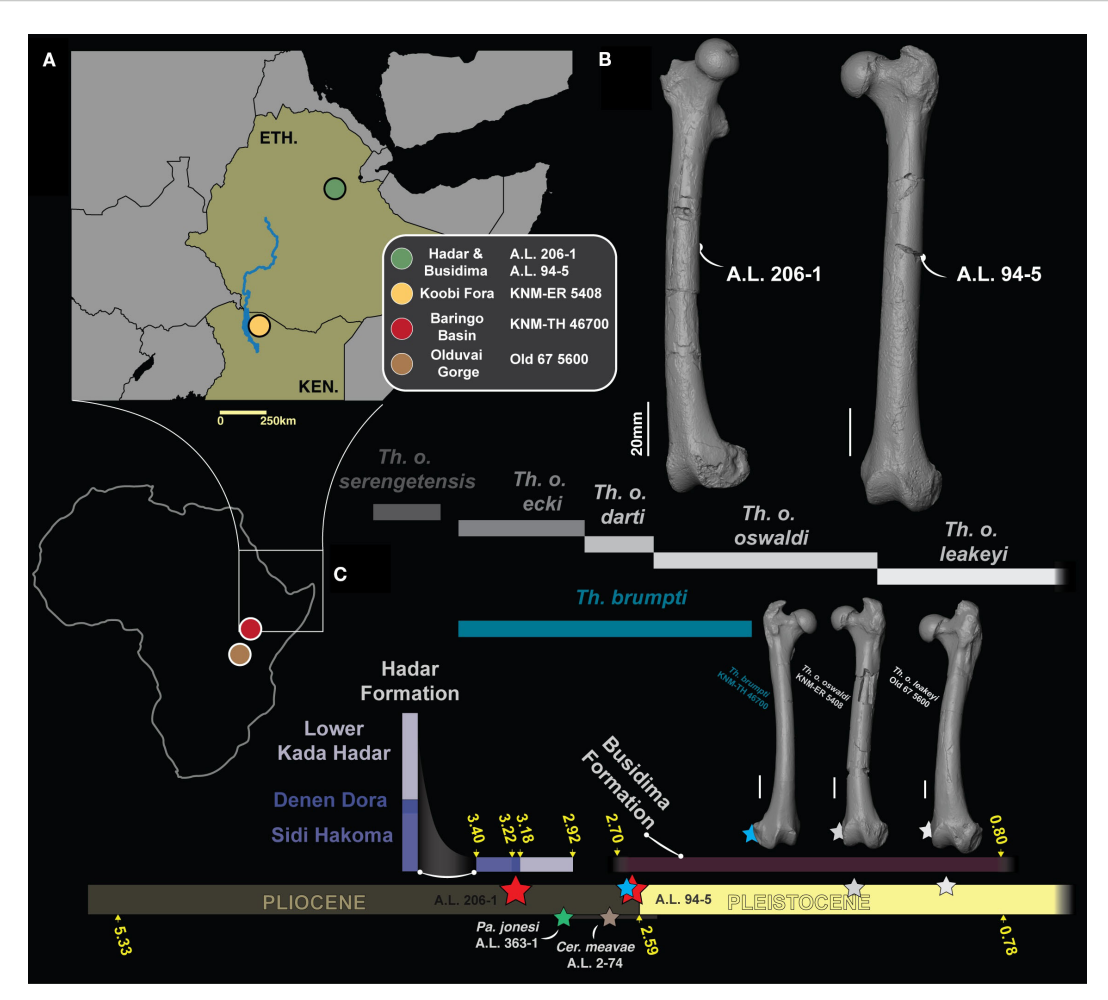


FIGURE 1
(A) Maps showing the geographic setting of fossiliferous formations and localities discussed in the text. (B) 3D generated surfaces of A.L. 206–1 and A.L. 94–5. (C) Chronostratigraphic frame of fossil *Theropithecus* along with 3D generated surfaces of *T. brumpti* KNM-TH 46700 (blue star), *T. o. oswaldi* KNM-ER 5408 (grey star) and *T. o. leakeyi* Old 67 5600 (white star). A.L. 206–1 and A.L. 94–5 are materialized by red stars while *Pa. jonesi* A.L. 363–1 and *Cer. meavae* A.L. 2–74 are materialized by a green and a brown star, respectively. The chronostratigraphic distribution of *Theropithecus* species follows Getahun et al. (2023).

#### Materials and methods

#### Paleontological sample

### The new fossils from the Afar Depression: A.L. 206–1 and A.L. 94–5

A.L. 206–1 is a right subcomplete femur discovered in 1974 in sediments from Submember 2 of the Denen Dora Member (DD-2, Hadar Formation) and initially attributed to *T. o. darti* by Krentz (1993) and Delson et al. (1993). However, no morphometric nor qualitative data were given to justify its taxonomic attribution. DD-2 is radiochronologically constrained between 3.24 Ma and 3.20 Ma (Behrensmeyer, 2008) and corresponds sedimentologically to fluvial or fluvio-deltaic sediments deposited on a deltaic plain (Campisano and Feibel, 2008). A.L. 94–5 is a left subcomplete femur discovered in a fossiliferous locality from the Lee Adoyta fault block in the Ledi-Geraru research area and is radiochronologically constrained between 2.67 Ma and 2.58 Ma (DiMaggio et al., 2015). A complete

description of both femora can be found in Supplementary Material S1.

# The other cercopithecid taxa from the Afar Depression: Parapapio cf. jonesi A.L. $363-1c\ \theta-1d$ and Cercopithecoides meavae A.L. 2-70, $-71\ \theta-74$

A.L. 363–1c and –1d are the right proximal and distal femur, respectively, of a partial male skeleton allocated to *Parapapio* and tentatively attributed to *Pa.* cf. *jonesi* (Frost and Delson, 2002). Craniodental remains include a partial skull and mandible, while the other postcranial remains include axial elements and a fifth metatarsal. The partial skeleton A.L. 363–1 was discovered in the upper part of the Kadar Hadar Member, in Submember KH-3, which is overlying the 2.95 Ma BKT-2 tuff (Campisano and Feibel, 2008). A.L. 2–70 and –71 are the left and right proximal femur and A.L. 2–74 is the left distal femur of the *Cercopithecoides meavae* colobine partial skeleton (Frost and Delson, 2002). The skeleton was

discovered in the Leadu locality but its chronostratigraphy is still uncertain, ranging from 3 Ma to 2.5 Ma.

# Contextual data on *Theropithecus brumpti* KNM-TH 46700, *Theropithecus* cf. oswaldi oswaldi KNM-ER 5408, and *Theropithecus* oswaldi leakeyi Old 67 5600

KNM-TH 46700 is a complete right femur of a partial skeleton of an older female *T. brumpti*, discovered from the Chemeron Formation in the Baringo Basin (Kenya). The skeleton was discovered in sediments dated, based on sedimentation rate, to 2.63 Ma (Gilbert et al., 2011). KNM-ER 5408 is a subcomplete left femur tentatively attributed to *T. o. oswaldi* given the absence of associated craniodental material (Jablonski et al., 2008). It was discovered in Area 103, in the Okote Member of the Koobi Formation, Kenya, and is radiochronologically constrained between 1.56 Ma and 1.48 Ma (Lepre and Kent, 2015). Old 67–5600 is a complete left femur from a male partial skeleton of *Theropithecus oswaldi leakeyi* discovered in the Upper Bed II sediments of the MCK (Margaret Cropper Korongo) II site at Olduvai and is dated between 1.74 Ma and 1.20 Ma (Szalay and Delson, 1979; Stanistreet, 2012; Frost et al., 2017).

#### Neontological dataset

Fossil Theropithecus were compared with all extant genera of papionins, except the rare Rungwecebus, encompassing extant African papionins (Papionina; n = 52 specimens) and Asian papionins (Macacina; n = 19 specimens). Only two species of Macaca (i.e., Macaca assamensis and Macaca nemestrina) were included as they represent relatively large Macaca species with body masses comparable to that expected for A.L. 206-1, and from which a substantial morphometric sample could be taken. Additional specimens (n = 26) of two medium-sized colobine taxa, Colobus guereza and Nasalis larvatus, were included to assess the hypothesis that A.L. 206-1 and A.L. 94-5 do not represent arboreal fossil colobine taxa such as Rhinocolobus turkanaensis, which is also recorded at Hadar (Frost and Delson, 2002). Data on extant specimens were collected from the Muséum National d'Histoire Naturelle (MNHN, Paris), Center for the Evolutionary Origins of Human Behavior (EHUB, Kyoto University), National Museums of Kenya (KNM, Nairobi), Bavarian State Collection for Zoology (ZSM, Munich), Smithsonian National Museum of Natural History (USNM, Washington), Natural History Museum, London, United Kingdom (NHMUK) and PALEVOPRIM laboratory (University of Poitiers).

Functionally, this sample includes taxa with terrestrial and arboreal substrate preferences such as *Papio* (Jolly, 2016b) and *Lophocebus* (Kingdon and Groves, 2016a), including taxa with mixed substrate preferences like *Cercocebus* (Groves and Butynski, 2016). It also includes arboreal climbers, represented by *Ma. assamensis* (Hirasaki et al., 2019) and *Colobus guereza* (Kingdon and Groves, 2016b), arboreal leapers with *Lophocebus* (Groves and Butynski, 2016), terrestrial walkers and runners with *Papio* (Jolly, 2016a) and terrestrial walkers, runners, and squatters

with *T. gelada* (Jolly, 2016b). See Pallas et al. (2023) for a summary of the locomotor behaviors of extant papionins.

## 3D scanning and femur alignments prior to morphometry

We obtained 3D data for A.L. 206–1 and A.L. 94–5 using an Artec Space Spider surface scanner while 3D data for *T. brumpti* (KNM-TH 46700), *T. cf. o. oswaldi* (KNM-ER 5408) and *T. o. leakeyi* (Old 67 5600) were generated with an EinScan Pro 2X surface scanner. Three-dimensional data for extant cercopithecids were obtained using surface scanners (Artec Space Spider and EinScan 2X) and photogrammetry (Panasonic DC-GX9). Information on data acquisition type can be found in Supplementary Material S2.

Prior to morphometry, all femora were aligned using MeshLab (Cignoni et al., 2008). We placed the center of the X, Y, Z orthonormal reference axes approximately at the level of the femoral mid-diaphysis. Femora were rotated so that the X axis was aligned with the femoral biepicondylar axis.

#### Linear morphometry

We collected n = 17 linear measurements using the landmarks presented and defined in Supplementary Materials S1, S3–5. All linear measurements were acquired from 3D models using Avizo and were acquired by a single operator (L.P.). Raw data can be accessed on Supplementary Table S2.

#### Body masses predictions

Body masses were estimated using the Ruff (2003) equation based on the superoinferior diameter of the femoral head. Regression equations used by Ruff (2003) were generated irrespective of sex for cercopithecines (y=2.389x-4.541) and colobines (y=2.424x-4.684) and were used here for extant and fossil specimens. Using the general equation rather than the sexspecific equation is relevant given the uncertain sex attribution of A.L. 94–5 and A.L. 206–1 (Supplementary Material S1).

#### 2D geometric morphometric

We obtained external contours of cross-sections at 75%, 50%, and 25% of the femoral biomechanical length (BL) using Avizo. We used tpsDig (Rohlf, 2006) to digitize landmarks (n=2) and semilandmarks (n=75). Section outlines were analyzed using landmarks placed at the most anterior and posterior points of the cross section, respectively, while semilandmarks were placed and distributed equidistantly along the outline of the cross-section.

Femoral curvature was assessed using 2D geometric morphometric by digitizing n = 3 landmarks and n = 75

semilandmarks along the anterior surface of the diaphysis (Supplementary Material S3). Landmarks and semilandmarks were digitized using tpsDig (Rohlf, 2006) on photographs of lateral views captured with Avizo. Landmarks were placed at the 75%, 50% and 25% of the biomechanical length of the femur while n = 75 equidistant semilandmarks were placed on the anterior edge of the diaphysis (Supplementary Material S3).

Prior to multivariate analysis, we computed a generalized Procrustes alignments of the landmarks and semilandmarks coordinates using the gpa function of geomorph (Adams et al., 2024) in R v.4.4.1 (R Core Team, 2024). This step consists in the alignment, rotation, and scaling of coordinates to ensure the retention of shape information only.

#### Morphometric ratios

To assess shape differences between taxa, we computed n=12 morphometric ratios that quantify the superoinferior robustness of the neck, the anteroposterior robustness of the femoral neck, the anteroposterior expansion of the femoral head, the relative length of the iliopsoas lever arm, the relative depth, height and width of the patellar groove, the relative anteroposterior depth of the lateral condyle, the depth differential of the lateral and medial condyle, the relative mediolateral width of the medial condyle, the relative mediolateral width of the intercondylar notch and the biepicondylar dimension.

Apart from the depth differential of the lateral and medial condyle ratio that represent the depth of the medial condyle divided by that of the lateral condyle, all ratios represent linear measurements divided by the geometric mean (GM) computed on the n = 17 linear measurements (Supplementary Material S5).

All ratios are biomechanically and/or taxonomically relevant, as previously reviewed in Pallas et al. (2023). The notable addition compared to Pallas et al. (2023) is the distal extension of the lesser trochanter which is linked with the lever arm length of the iliopsoas muscle group, a major flexor of the hip and external rotator (Rodman, 1979; Lifshitz et al., 2020). We briefly summarized here the relevance of all other ratios. The relative superoinferior height of the femoral neck is related to resistance in bending loads set in the coronal plane due to the weight-bearing functions of the hip (Fleagle and Meldrum, 1988; Nakatsukasa, 1994; Fleagle and Simons, 1995; Cooke and Tallman, 2012) while the mediolateral width of the femoral head is related to mobility of the coxofemoral (hip) joint and stress dissipation (Ward, 1993; Bouma et al., 2013). The depth, height and width of the patellar groove is related with mobility and load dissipation at the patellofemoral (knee) joint (Tardieu, 1983; Ford, 1988; Gebo and Sargis, 1994; Nakatsukasa, 1994; Madar et al., 2002). The depth of the femoral condyles is linked with mobility of the knee, notably its flexion/extension and abduction ability while the width of the femoral condyles is reflective of load dissipation of the knee given specific knee positions (Tardieu, 1983; Nakatsukasa, 1994; Madar et al., 2002). The intercondylar notch and biepicondylar widths are related with knee rotational abilities (Nakatsukasa, 1994; Pallas et al., 2023).

### Linear regression of femoral length on body mass

As the scaling of femoral length on body mass discriminates extant papionins (Strasser, 1992), we regressed the natural logarithm of the biomechanical femoral length of extant and fossil cercopithecids on their inferred body masses. We computed a linear regression using the lm function of the stats package (R Core Team, 2024) and visualized results using a bivariate plot of femoral length over body mass and a boxplot of the model residuals.

#### Multivariate analyses

We performed a principal component analysis (PCA) to order variation and visualize our morphometric data. Five datasets were generated and subjected to PCA: *i)* linear morphometric data and Procrustes coordinates of cross-sections at *ii)* 75%, *iii)* 50%, and *iv)* 25% of femoral biomechanical lengths as well as *v)* Procrustes coordinates of femoral curvature.

All data were scaled and centered prior to PCA and then subjected to PCA using the function prcomp of stats (R Core Team, 2024). Principal component (PC) scores were visualized using biplots and boxplots. For linear dimensions, data were transformed using the log-shape ratio method prior to inclusion in the PCA (Mosimann, 1970).

## Statistical modelling and hierarchical clustering

To assess the phenetic affinity of fossil femora based on linear morphometric data, we computed a linear discriminant analysis (LDA) with the lda function of MASS (Venables and Ripley, 1997) on the femoral dimensions scaled using the log-shape ratio method (Mosimann, 1970). Class memberships were defined as equiprobable for each extant taxon prior to LDA. The accuracy of the model was assessed using the Leave One Out Cross-Validation (LOOCV) method by computing a confusion matrix using the confusionMatrix function of caret (Kuhn, 2008).

In addition to the LDA generated on linear data, we explored the phenetic affinity of the fossil femora to extant cercopithecid genera using a hierarchical clustering established on mean values of morphometric ratios and mean values of PC scores from selected multivariate analyses. To this end, we retained 10 morphometric ratios that permitted to discriminate extant geladas from other cercopithecids (i.e., femoral head anteroposterior expansion, femoral neck superoinferior robustness, femoral neck anteroposterior robustness, relative iliopsoas lever arm length, relative intercondylar notch width, relative biepicondylar width, condylar depth differential, relative patellar groove width, relative patellar groove height, and relative patellar groove depth), in addition to the residual values of the regression of femoral length on body mass as well as the scores of the first PCs for the 2D geometric morphometric PCA of the cross-sectional shape and

curvature of the femur. We computed mean data for these variables for each genus, which where then scaled and centered, and we computed a distance matrix, based on Euclidean distance, using the dist function of stats (R Core Team, 2024). We computed a hierarchical clustering following the Ward clustering method [following the algorithm of Murtagh and Legendre (2014)], which minimizes the total-within cluster variance, using the hclust function of stats (R Core Team, 2024).

We computed analysis of variance (ANOVA) and multivariate analysis of variance (MANOVA) to evaluate whether extant taxa can be significantly discriminated based on morphometric ratio values and PC scores, respectively. We set the levels of significance of our tests at 5%. ANOVA were computed using the aov function of stats and MANOVA using the manova function (R Core Team, 2024). Prior to ANOVA, we tested the following assumptions: i) there is no significant differences in data normality between the dependent variables and ii) there is no significant differences in data homoscedasticity between the dependent variables (Table 1). Normality of the model residuals was assessed using the Shapiro-Wilk test with the shapiro.test function of stats (R Core Team, 2024). Homoscedasticity of the data was evaluated using the bartlett.test function of stats (R Core Team, 2024). A particular attention was given to homoscedasticity as ANOVA is robust to non-normality of the data. In cases where we failed to validate homoscedasticity, we used the non-parametric Kruskall-Wallis and permutational MANOVA (PERMANOVA) tests. The Kruskall-Wallis test was applied using the kruskal.test function of stats and PERMANOVA using the adonis function of vegan (Oksanen et al., 2001). We ran post-hoc tests following MANOVA and PERMANOVA. For ANOVA, we used the Tukey's Honest Significant Difference (HSD) with the TukeyHSD function of stats. For Kruskall-Wallis, we used the Dunn's Test with the dunnTest function of FSA (Ogle et al., 2023).

#### Results

# Principal component analysis based on the complete morphometric dataset

The PC1-PC2 biplot accounts for ca. 36% of the variance (Figure 2). Extant geladas show a combination of negative PC1 scores and positive PC2 scores. Such a combination is also seen in A.L. 206–1, *T. o. oswaldi* (KNM-ER 5408) and *T. o. leakeyi* (Old 67 5600). In contrast, A.L. 94–5 and *T. brumpti* (KNM-TH 46700) present negative PC2 scores and group close to *Macaca* for the former, and *N. larvatus* for the latter. Negative PC1 scores are driven by femoral head dimensions (anteroposterior and superoinferior), the width of the intercondylar notch and the anteroposterior dimension of the neck while positive PC1 scores are driven by patellar groove depth and anteroposterior diameter at mid-diaphysis. Positive PC2 scores are influenced by the length of the iliopsoas lever arm, the depth of the medial and lateral condyles, and the width of the patellar groove. Negative PC2 scores are due to neck dimensions (anteroposterior and superoinferior) and patellar groove depth.

The PC1-PC3 biplot accounts for ca. 32% of the variance (Figure 2). Extant geladas show positive or slightly negative scores on PC3, as is the case for all fossil *Theropithecus*. The highly positive scores of A.L. 94–5 and *T. o. oswaldi* are to be noticed, as they fit with *Ma. assamensis* in PC3 scores. Positive PC3 scores are driven by iliopsoas lever arm length as well as anteroposterior and mediolateral dimensions at midshaft while negative PC3 scores are driven by the height of the patellar groove and the width of the lateral condyle.

Extant cercopithecid taxa can be statistically discriminated using the first three PC scores (Table 2). PC1 scores notably permit the discrimination of *T. gelada* from all other taxa (Supplementary Material S6). PC2 scores significantly discriminates *T. gelada* from all other taxa except *Mandrillus* and *Papio* (Supplementary Material S6). Lastly, PC3 scores significantly distinguish *T. gelada* from all extant taxa but colobines and *Papio* (Supplementary Material S6).

### Linear discriminant analysis on the complete morphometric dataset

The discrimination accuracy of the LDA is modest, with an accuracy of ca. 65%. As for the PCA, fossil Theropithecus show a similar combination of scores to that of T. gelada on the LD1-LD2 biplot (65.5% of the variance), with positive LD1 scores and moderately positive or negative LD2 scores (Figure 3). A.L. 94-5 and A.L. 206-1 nonetheless present higher LD2 scores compared with other extant and fossil Theropithecus. For the LD3 axis (12.6% of the variance), T. o. oswaldi (KNM-ER 5408) and T. o. leakeyi (Old 67 5600) presents a much higher LD3 scores compared to other Theropithecus and clusters with Mandrillus. Positive LD1 scores are mostly influenced by the length of the iliopsoas lever arm and the anteroposterior dimension of the neck while negative scores are influenced by femoral length. Positive LD2 scores are influenced by iliopsoas lever arm length and negative LD2 scores by the mediolateral dimension of the lateral condyle, the anteroposterior dimension of the head, and the superoinferior dimension of the patellar groove. Positive LD3 scores are impacted by the mediolateral dimension of the diaphysis at mid-length and by the depth of the lateral condyle while negative LD3 scores reflects femoral length.

Overall, the positive scores of extant and fossil *Theropithecus* on LD1, the main axis of variation, illustrate their short femur, long iliopsoas lever arm length, and anteroposteriorly expanded femoral neck.

# Principal component analysis and linear discriminant analysis of the femoral epiphyses

The sparse morphometric dataset used here is limited to dimensions of the proximal and distal epiphyses, permitting to compare A.L. 206–1 and A.L. 94–5 with *Pa. jonesi* (A.L. 363–1) and *Cer. meavae* (A.L. 2–74).

TABLE 1 Results of One-way ANOVA for the morphometric ratios.

	Normality (Shapiro-Wilk)	Homoscedasticity (Bartlett)	Model (ANOVA or Kruskal-Wallis)
Femoral neck robustness	W = 1, p.val = 0.01	$K^2 = 14$ , p. val = 0.07	Kruskal-Wallis $X^2 = 26$ , p. val = 0.001
Lever arm length of illiopsoas	W = 1, p.val = 0.2	$K^2 = 12$ , p.val = 0.1	ANOVA F = 19, p. val < 0.001
Medial condyle width	W = 1, p.val = 0.1	$K^2 = 13$ , p.val = 0.1	ANOVA F = 4.95, p. val < 0.001
Lateral condyle depth	W = 1, p.val = 1	$K^2 = 6$ , p.val = 0.6	ANOVA F = 3.30, p. val < 0.001
Biepicondylar width	W = 1, p.val = 0.2	K <sup>2</sup> = 20, p.val = 0.01	Kruskal-Wallis $X^2 = 34$ , p. val = 0.001
Patellar groove depth	W = 1, p.val = 0.09	$K^2 = 18$ , p.val = 0.02	Kruskal-Wallis $X^2 = 48$ , p. val < 0.001
Patellar groove width	W = 1, p.val = 0.3	$K^2 = 15$ , p.val = 0.06	ANOVA F = 5.85, p. val < 0.001
Femoral head width	W = 1, p.val = 0.9	$K^2 = 5$ , p.val = 0.70	ANOVA F = 7.35, p. val < 0.001
Intercondylar notch width	W = 1, p.val = 0.4	$K^2 = 4$ , p.val = 0.80	ANOVA F = 5.29, p. val < 0.001
Patellar groove height	W = 1, p.val = 1	K <sup>2</sup> = 17, p.val = 0.03	Kruskal-Wallis $X^2 = 23,$ p. val = 0.003
Depth differential of the condyles	W = 1, p.val = 0.6	$K^2 = 11$ , p.val = 0.20	ANOVA F = 8.68, p. val < 0.001
PC1 scores femoral curvature	W = 1, p.val = 0.3	$K^2 = 6$ , p.val = 0.60	ANOVA F = 2.11, p. val < 0.05

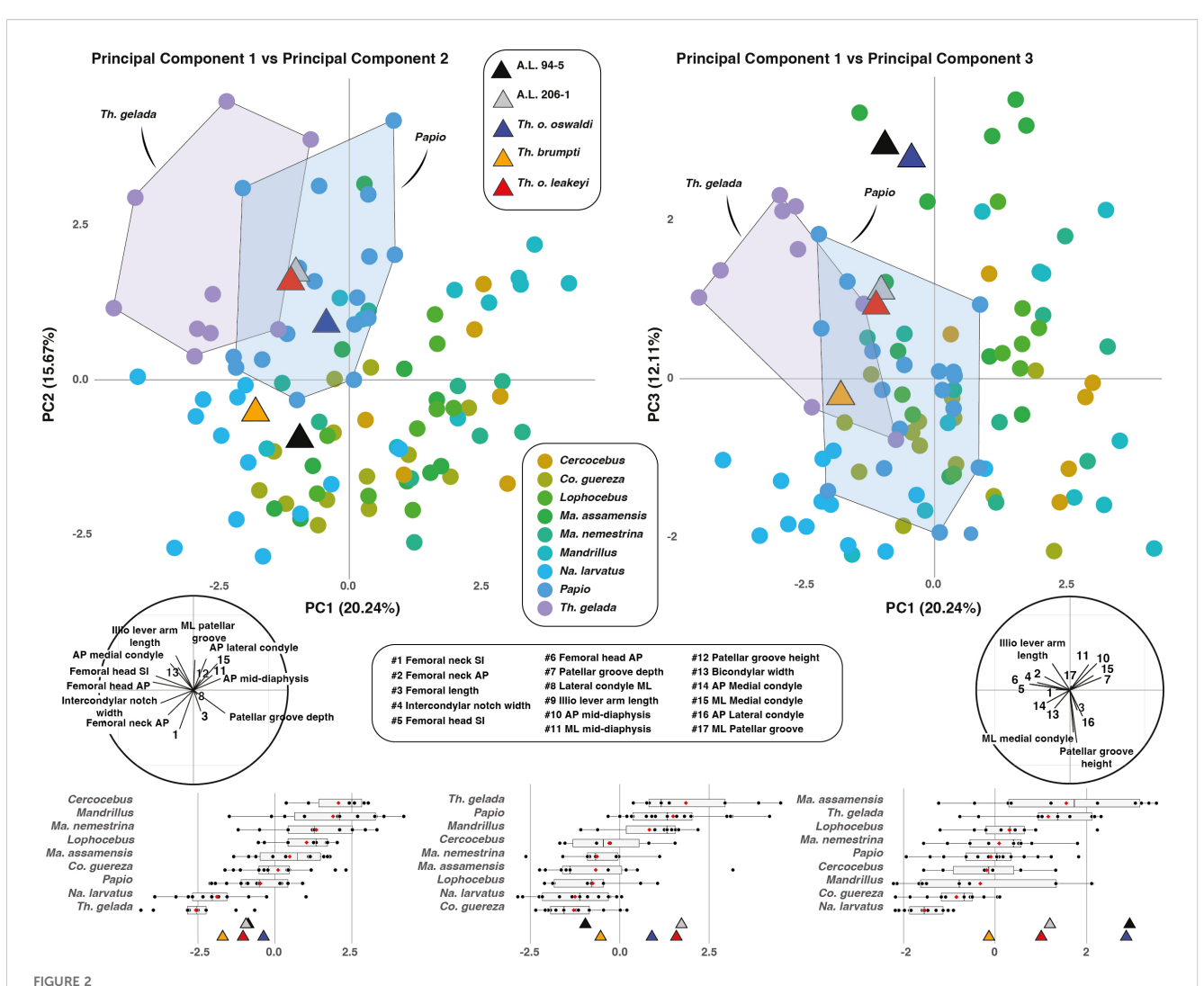
Bold text indicates significant p-values.

Overall, the multivariate analyses of the proximal and distal epiphyseal dimensions permit to distinguish cf. Pa. jonesi from fossil Theropithecus as well as A.L. 206–1 and A.L. 94–5 (Supplementary Material S7). The putative Pa. jonesi femur notably presents a deep patellar groove and a wide medial condyle, like the more arboreal papionins Ma. assamensis and Macaca nemestrina. It is much more complicated to conclude for the fossil colobine Cer. meavae given its proximity with extant and fossil papionins on PCs and LDs scores. The fossil colobine Cer. meavae is notably sharing with extant papionins Papio and T. gelada a longer iliopsoas lever arm length and an anteroposteriorly wide femoral head. However, Cer. meavae present a neck much more gracile than that of A.L. 94–5 on one hand, and a reduced biepicondylar width and less longer (anteroposteriorly) medial

condyle than that of A.L. 206–1 on the other hand, supporting a separate taxonomic assignment of *Cer. meavae* for the subcomplete femora.

#### Allometry of femoral length

The femur of *T. gelada* scales differently compared to other cercopithecids, including *Papio* (Figure 4A). Femora of *T. gelada* are shorter for any given body mass compared with that of *Papio*, as observed by negative residuals (Figure 4B). A.L. 206–1 and A.L. 94–5, along with other fossil *Theropithecus*, present short femur and negative residuals comparable to that of extant geladas (Figure 4B).



PC1-PC2 biplot (left panel) and PC1-PC3 biplot (right panel) of extant and fossil cercopithecids. Correlation circles are visible on the bottom left and right corners of the PC1-PC2 biplot and PC1-PC3 biplot, respectively. Boxplots of PC scores for PC1, PC2 and PC3 are given in the lower panel with median (black bar), mean (red losange), first quartile and third quartile.

# Proximal femur (posterior and inferior view)

A distally placed lesser trochanter (high iliopsoas lever arm length) is visible in A.L. 206–1 and A.L. 94–5, as illustrated by their high iliopsoas lever arm length relative to size (i.e., GM) (Figure 5). High values, and hence long lever arm length, are also observed in *T. gelada* (Supplementary Material S8), with significant differences from all other cercopithecids (Supplementary Material S9), and notably with the short lever arm length and proximally placed lesser trochanter of *Co. guereza*. While A.L. 206–1 and A.L. 94–5 conform with the morphological pattern of extant *T. gelada*, the large-sized fossil *Theropithecus* species (*T. brumpti*, *T. o. oswaldi* and *T. o. leakeyi*) are more like *Papio* than *T. gelada* (Figure 5).

The superoinferior diameter of the neck is extremely large relative to size in A.L. 94–5 compared to A.L. 206–1, which has a more gracile neck (Figure 5; Supplementary Material S8). Apart from large values of *Na. larvatus*, there are large overlaps in ranges

of variation among cercopithecids. The large-sized fossil *Theropithecus* species have a superoinferiorly robust neck like that of *Na. larvatus*, but more gracile than that of A.L. 94–5.

The femoral head of A.L. 206–1 and A.L. 94–5 is not particularly expanded anteroposteriorly relative to its size (Figure 5). It contrasts with the anteroposteriorly expanded femoral head of *T. gelada* and *Papio* (Figure 5; Supplementary Material S8). A much narrower femoral head is seen in *Ma. nemestrina* and *Cercocebus*. The *T. brumpti* KNM-TH 46700, *T. o. oswaldi* KNM-ER 5408 and *T. o. leakeyi* Old 67–5600 specimens all have an anteroposteriorly expanded femoral head, in contrast to the Afar femora, and are consistent with that of extant *T. gelada*.

#### Distal femur (posterior view)

A larger medial condyle relative to size is seen in A.L. 206-1 compared to A.L. 94-5 (Figure 6; Supplementary Material S10). A

TABLE 2 Result of the multivariate ANOVA on linear morphometric data.

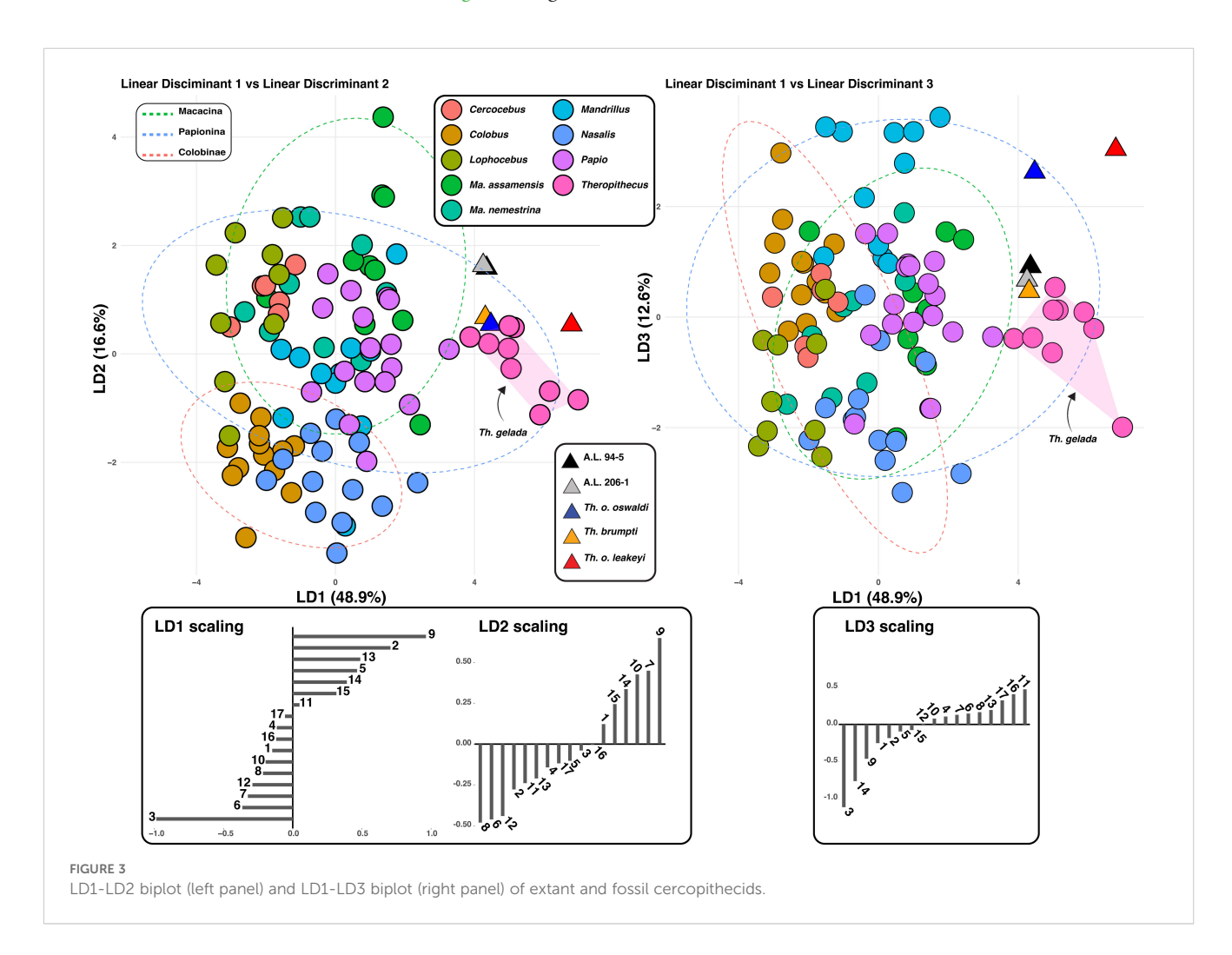
	Multivariate normality (Shapiro-Wilk multivariate extension)	Homogeneity of covariance	Model (MANOVA or Kruskal-Wallis)
PCA Scores Linear Morphometry	p. val = 0.07	p. val = 0.015	MANOVA PC1 F val. = 15.9, p. val < 0.001
			MANOVA PC2 F val. = 11.2, p. val < 0.001
			MANOVA PC3 F val. = 7.72 p. val < 0.001

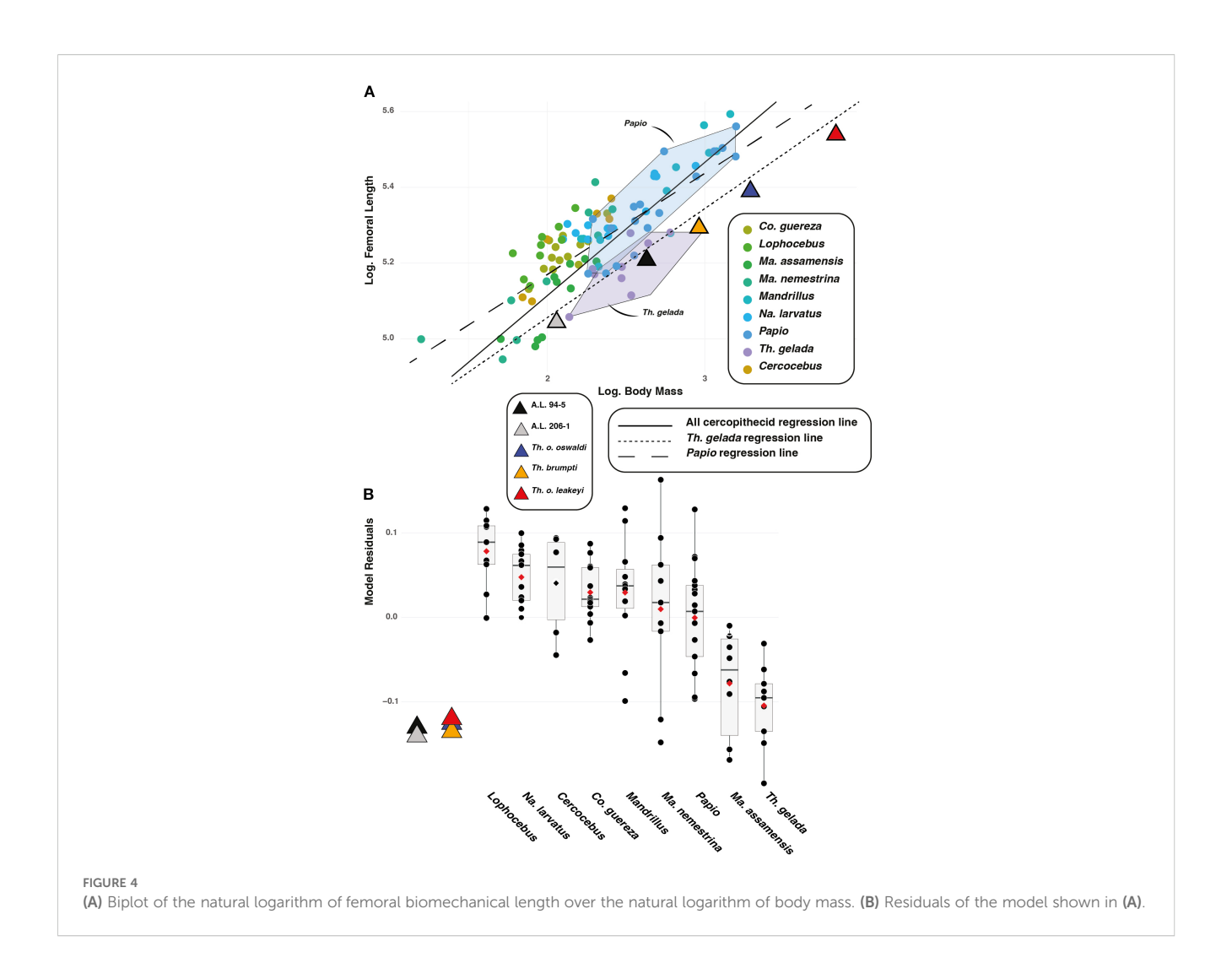
Bold text indicates significant p-values.

relatively large medial condyle is characteristic of *Mandrillus* and *Macaca* while a narrow medial condyle is typical of *Na. larvatus*. While extensive overlaps are seen among extant cercopithecids regarding this trait, *Mandrillus*, *Macaca* and *Na. larvatus* can be significantly distinguished in this feature (Supplementary Material S9). A.L. 94–5 falls near the mean value of *Na. larvatus* while A.L. 206–1 best conforms with other large-sized African papionins. Other fossil *Theropithecus* (Supplementary Material S10) show values most like *Papio* and *Mandrillus* (Figure 6).

The intercondylar notch of A.L. 206–1 is extremely wide relative to size and is much wider than that of A.L. 94–5 (Figure 6). *T. gelada* 

also exhibit a large intercondylar notch (Figure 6; Supplementary Material S10), contrasting markedly with the narrow intercondylar notch of *Mandrillus* and *Cercocebus*. Both *T. gelada* and *Mandrillus* can be significantly discriminated from other cercopithecids in this aspect (Supplementary Material S9). A.L. 206–1 fits in the third quartile of *T. gelada* while A.L. 94–5 falls near the *Papio* mean value (Figure 6). While *T. brumpti* KNM-TH 46700 and *T. o. leakeyi* Old 67–5600 fits within the interquartile range of *Papio*, *T. o. oswaldi* KNM-ER 5408 has a much narrower intercondylar notch and falls in the interquartile range of *Mandrillus* (Figure 6; Supplementary Material S10).





The distal epiphysis of A.L. 206–1 is very wide relative to size while that of A.L. 94–5 is much narrower (Figure 6). An extremely wide distal epiphysis is characteristic of *T. gelada*, with barely any overlap in interquartile range with other considered cercopithecids, and as such, have significant differences in index values (Supplementary Material S9). The wide distal epiphysis of A.L. 206–1 is comparable to that of *T. gelada* while that of A.L. 94–5 is most like *Cercocebus* and *Lophocebus*. A.L. 94–5 also shares a narrow distal epiphysis with *T. o. oswaldi* KNM-ER 5408 while the relatively wide distal epiphysis of A.L. 206–1 is also seen in *T. brumpti* KNM-TH 46700 and *T. o. leakeyi* Old 67 5600 (Figure 6; Supplementary Material S10).

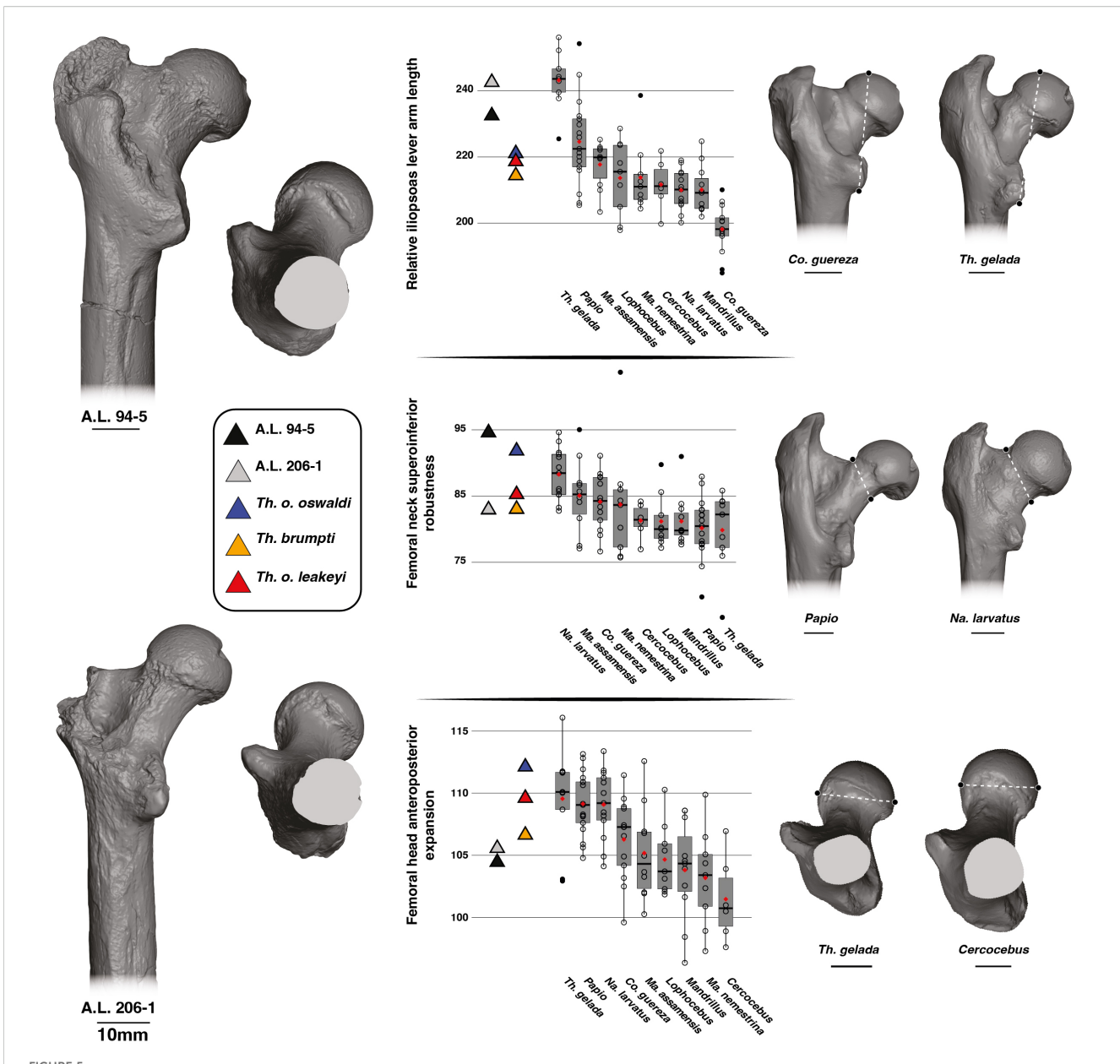
#### Distal femur (inferior view)

The patellar groove of A.L. 206–1 is narrower relative to size than that of A.L. 94–5 (Figure 7). A relatively narrow patellar groove is commonly seen in *Na. larvatus* while a wider one is characteristic of *T. gelada* (Supplementary Material S5). The width of the patellar groove of A.L. 94–5 is similar to values obtained for *T. gelada*, *Papio* 

and *Mandrillus* and is also similar to *T. o. oswaldi* KNM-ER 5408 (Supplementary Material S11). The narrow patellar groove of A.L. 206–1 is in line with the morphology of *T. brumpti* KNM-TH 46700 and *T. o. leakeyi* Old 67 5600, in addition to fitting close to the mean value of *Ma. nemestrina* and *Na. larvatus*.

The lateral condyle of A.L. 206–1 is elongated anteroposteriorly while that of A.L. 94–5 is comparatively shorter (Figure 7). Deep lateral condyles are observed in all non-*Theropithecus* African papionins (Figure 7; Supplementary Material S11). Deep lateral condyles are also seen in *T. brumpti* KNM-TH 46700 and *T. o. leakeyi* Old 67 5600, while a shorter condyle is observed in *T. o. oswaldi* KNM-ER 5408 (Figure 7; Supplementary Material S11).

A moderate condyle depth differential is observed in A.L. 206–1 and A.L. 94–5, with values fitting with the lower range of variation of extant *T. gelada* (Figure 7). This translates an elongated medial condyle relative to the lateral condyle. The reverse is true for *Mandrillus* and *Cercocebus*, with, on average, a longer lateral condyle relative to the medial condyle (Figure 7). A much-pronounced condyle depth differential is seen in other fossil *Theropithecus* (Figure 7; Supplementary Material S11).



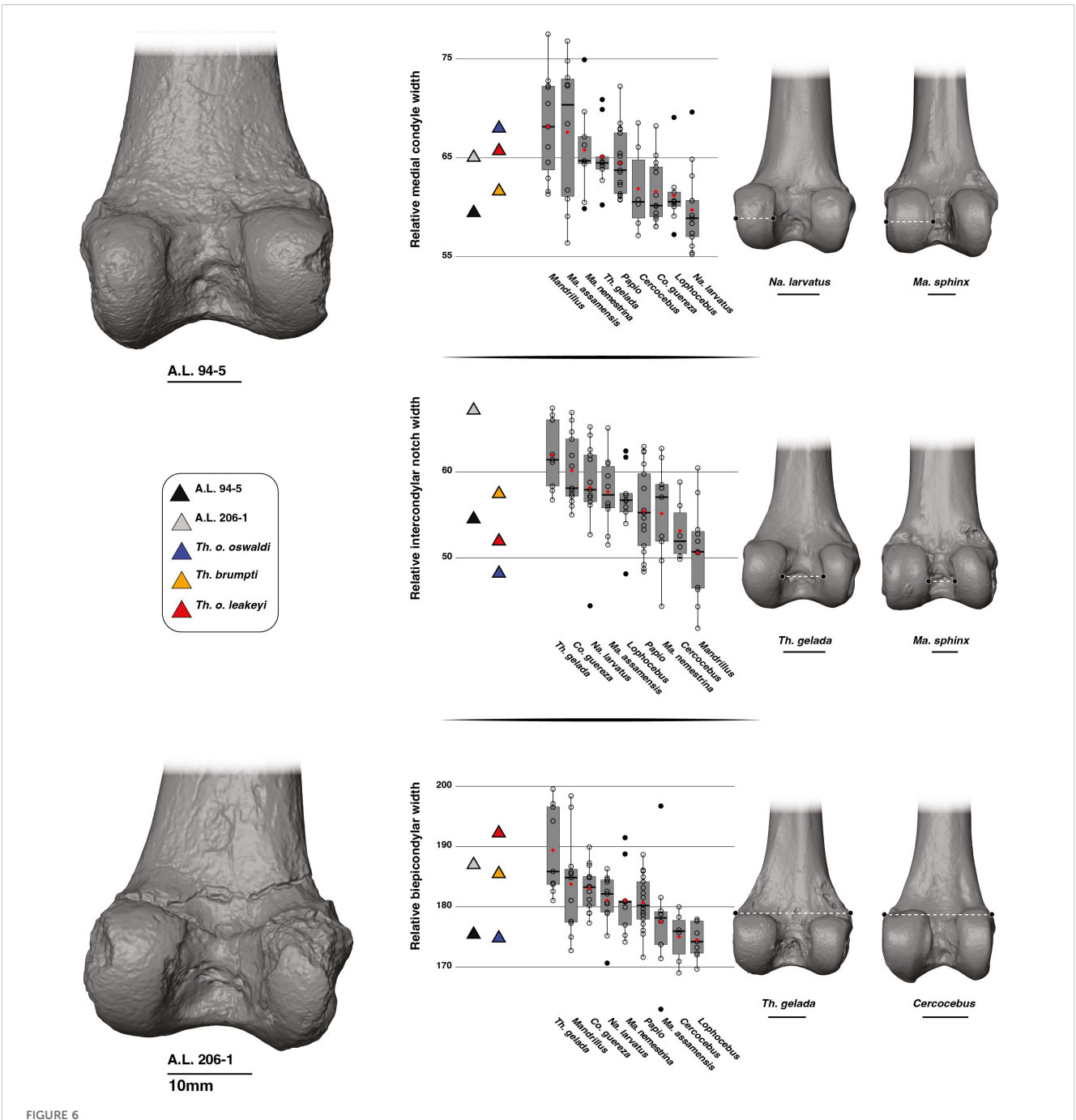
3D generated surfaces of the proximal epiphysis of A.L. 94–5 and A.L. 206–1 in posterior and inferior views (left panel) along with boxplots of the iliopsoas lever arm length, femoral neck height, and femoral head width standardized by the geometric mean (GM) for extant and fossil cercopithecids on the central panel. Boxplots with median (black bar), mean (red losange), first quartile and third quartile. 3D generated surfaces of extant cercopithecids showing extreme morphologies for each index is visible on the right panel.

#### Distal femur (anterior view)

A proximodistally short patellar groove relative to GM is observed in A.L. 206–1 and A.L. 94–5, a feature also observed in *T. gelada* (Figure 8; Supplementary Material S12). Extant geladas, along with *Macaca*, show the lowest patellar groove among the considered extant cercopithecids, contrasting with *Na. larvatus*, *Mandrillus* and *Cercocebus* (Figure 8). However, the range of variation is very wide in *Ma. assamensis* and overlaps extensively with that of other taxa. The patellar groove of *T. brumpti* KNM-TH 46700, *T. o. oswaldi* KNM-ER 5408 and *T. o. leakeyi* Old 67–5600 is

low relative to size and is consistent with that of A.L. 206–1, A.L. 94–5 and extant *T. gelada* (Figure 8; Supplementary Material S12).

The patellar groove is relatively shallow in A.L. 94–5 and A.L. 206–1 (Figure 8). An extremely shallow patellar groove is typical of *T. gelada* which can be significantly discriminated from other cercopithecids in this aspect (Supplementary Material S9). The opposite condition (a deep patellar groove) is observed in *Macaca*. The relative depth of the patellar groove of *T. brumpti* KNM-TH 46700, *T. o. oswaldi* KNM-ER 5408 and *T. o. leakeyi* Old 67–5600 is slightly higher than that of both Afar femora and overall, fits within the range of variation of *Papio* and *Mandrillus* and is



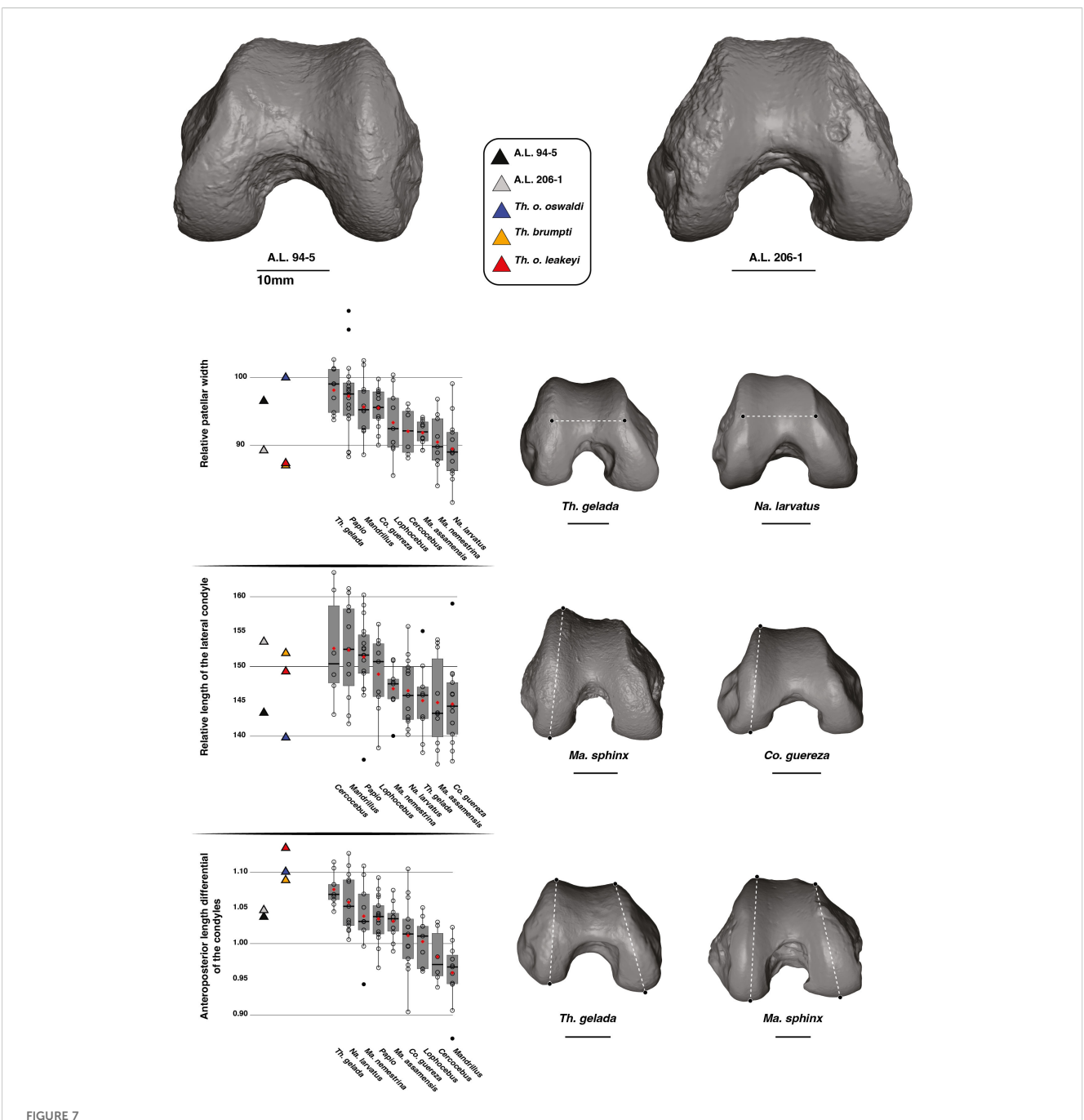
3D generated surfaces of the distal epiphysis of A.L. 94–5 and A.L. 206–1 in posterior view (left panel) along with boxplots of the medial condyle width, intercondylar notch width, and biepicondylar width standardized by the geometric mean (GM) for extant and fossil cercopithecids on the central panel. Boxplots with median (black bar), mean (red losange), first quartile and third quartile. 3D generated surfaces of extant cercopithecids showing extreme morphologies for each index is visible on the right panel.

deeper than that of extant *T. gelada* (Figure 8; Supplementary Material S12).

#### Femoral curvature

PC1 accounts for 83.45% of the variance and explain the overall curvature of the anterior aspect of the femoral shaft (Figure 9). PC2 is

not commented here given its low explanatory value compared to PC1 (12.3% vs. 83.45%, respectively). For PC1 scores, the femoral shafts of A.L. 206–1 and A.L. 94–5 are not strongly curved and overlap extensively with all the extant cercopithecids (Figure 9), which cannot be discriminated statistically (Supplementary Material S9). The femur of *T. o. oswaldi* KNM-ER 5408 is also only weakly curved and similar in this aspect to A.L. 206–1 and A.L. 94–5, but strikingly distinct from the highly curved femora of KNM-

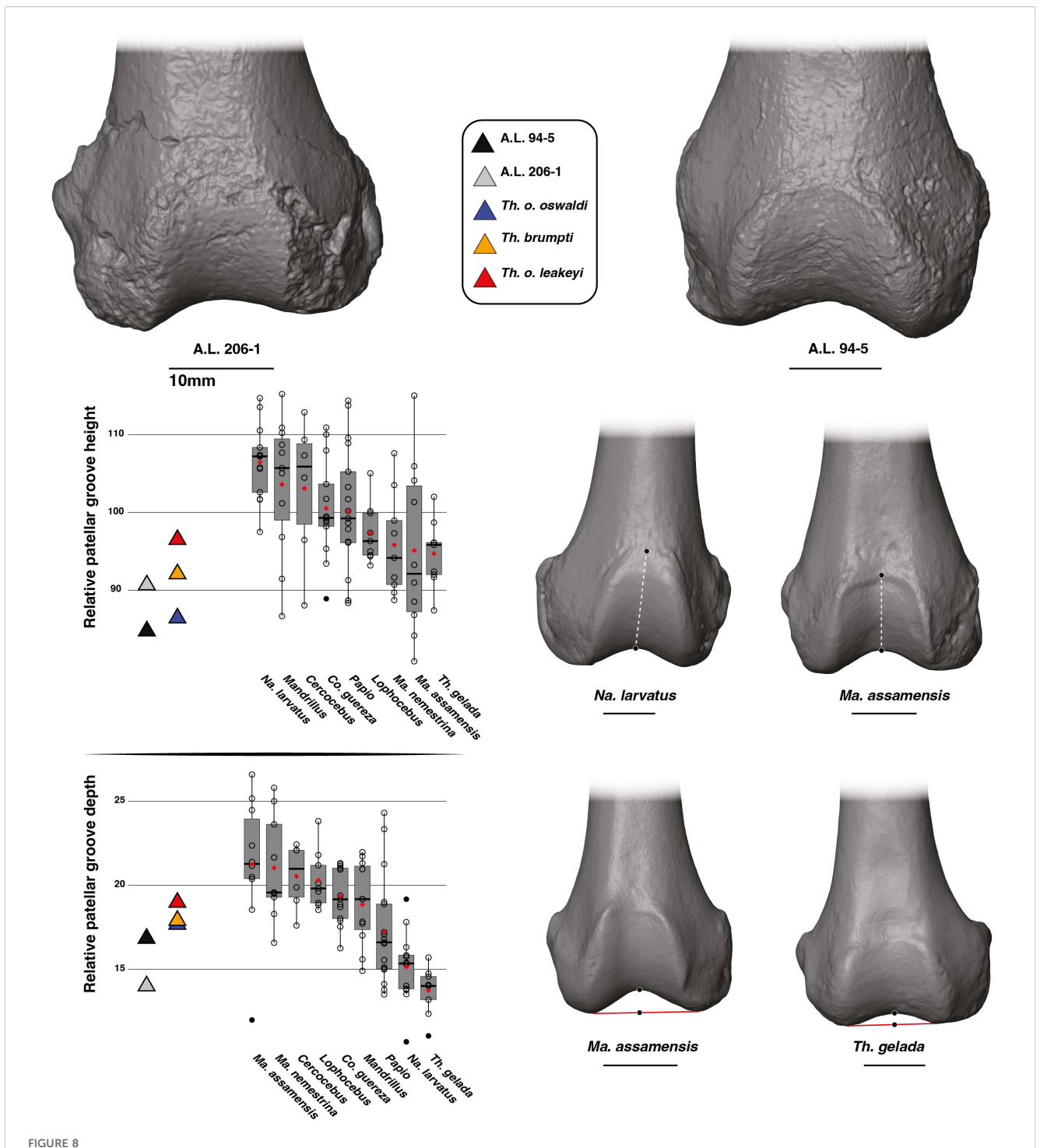


3D generated surfaces of the distal epiphysis of A.L. 94–5 and A.L. 206–1 in inferior view (left panel) along with boxplots of the patellar width and lateral condyle depth standardized by the geometric mean (GM) along with the depth differential of the condyles for extant and fossil cercopithecids on the central panel. Boxplots with median (black bar), mean (red losange), first quartile and third quartile. 3D generated surfaces of extant cercopithecids showing extreme morphologies for each index is visible on the right panel.

TH 46700 *T. brumpti* and *T. o. leakeyi* Old 67-5600 (Figure 9). The PC1 scores and femoral curvature of *T. brumpti* and *T. o. leakeyi* are unmatched among extant papionins. The femora of *Papio*, *T. gelada*, *Ma. nemestrina* and *Ma. assamensis* are, on average, more strongly curved than that of the other considered cercopithecids but we failed to detect significant differences in PC1 scores.

#### Femoral cross-sectional contours

On PC1 scores of the cross-section shape set at 75% of femoral BL, A.L. 206–1 and A.L. 94.5 present an anteroposteriorly extended proximal metaphysis as indicated by negative PC1 scores and are quite similar in shape and scores to that of *T. gelada* (Figure 10).

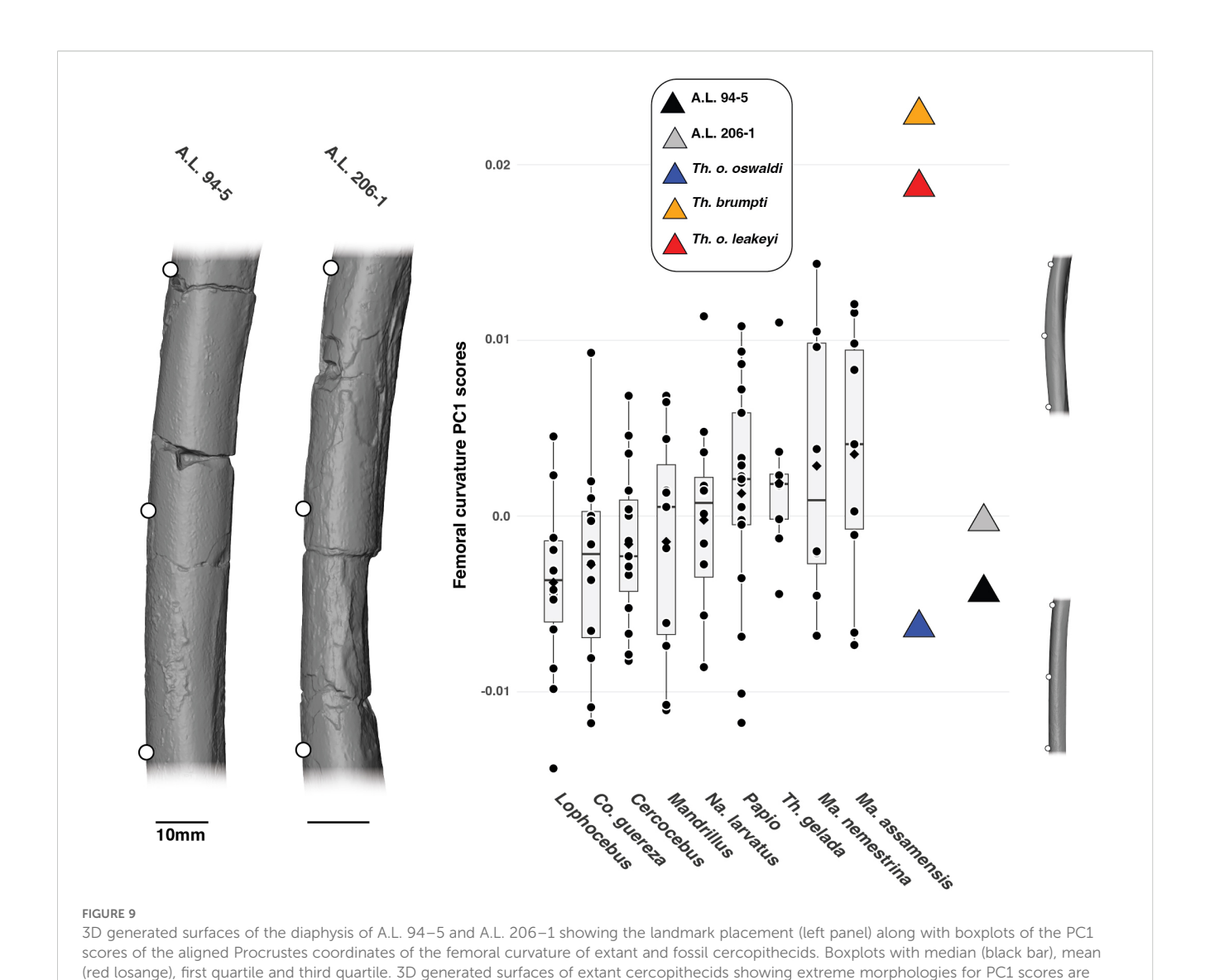


3D generated surfaces of the distal epiphysis of A.L. 94–5 and A.L. 206–1 in anterior view (left panel) along with boxplots of the patellar height and patellar depth standardized by the geometric mean (GM) for extant and fossil cercopithecids on the central panel. Boxplots with median (black bar), mean (red losange), first quartile and third quartile. 3D generated surfaces of extant cercopithecids showing extreme morphologies for each index is visible on the right panel.

The proximal metaphysis of *T. brumpti* KNM-TH 46700 and *T. o. oswaldi* KNM-ER 5408 are slightly more elliptical mediolaterally as indicated by their PC1 scores around zero. Overall, fossil *Theropithecus* are distinct from the mediolaterally elongated proximal femoral metaphysis of *Macaca* and *Mandrillus* and are more like *Papio* and *T. gelada*. The negative scores of A.L. 206–1

and A.L. 94–5 on PC2 scores align them with the colobines and *T. gelada* and reflects a poorly developed gluteal tuberosity.

In PCA of the cross-sectional shape at 50% of femoral BL, PC1 illustrates the anteroposteriorly elongated mid-diaphysis of A.L. 206–1 and A.L. 94–5, fitting with the positive PC1 scores of *Co. guereza* and *Lophocebus* but falling outside the negative scores of *T.* 



gelada (Figure 10). A wide range of variation is seen for the largesized fossil *Theropithecus* with negative, null, and positive PC1 scores. Contrary to PC1, all fossil *Theropithecus* show positive PC2 scores, indicating a poorly developed lateral margin of the vastus lateralis on the linea aspera. Fossil *Theropithecus* are quite distinct in this aspect from *Papio* and *T. gelada*.

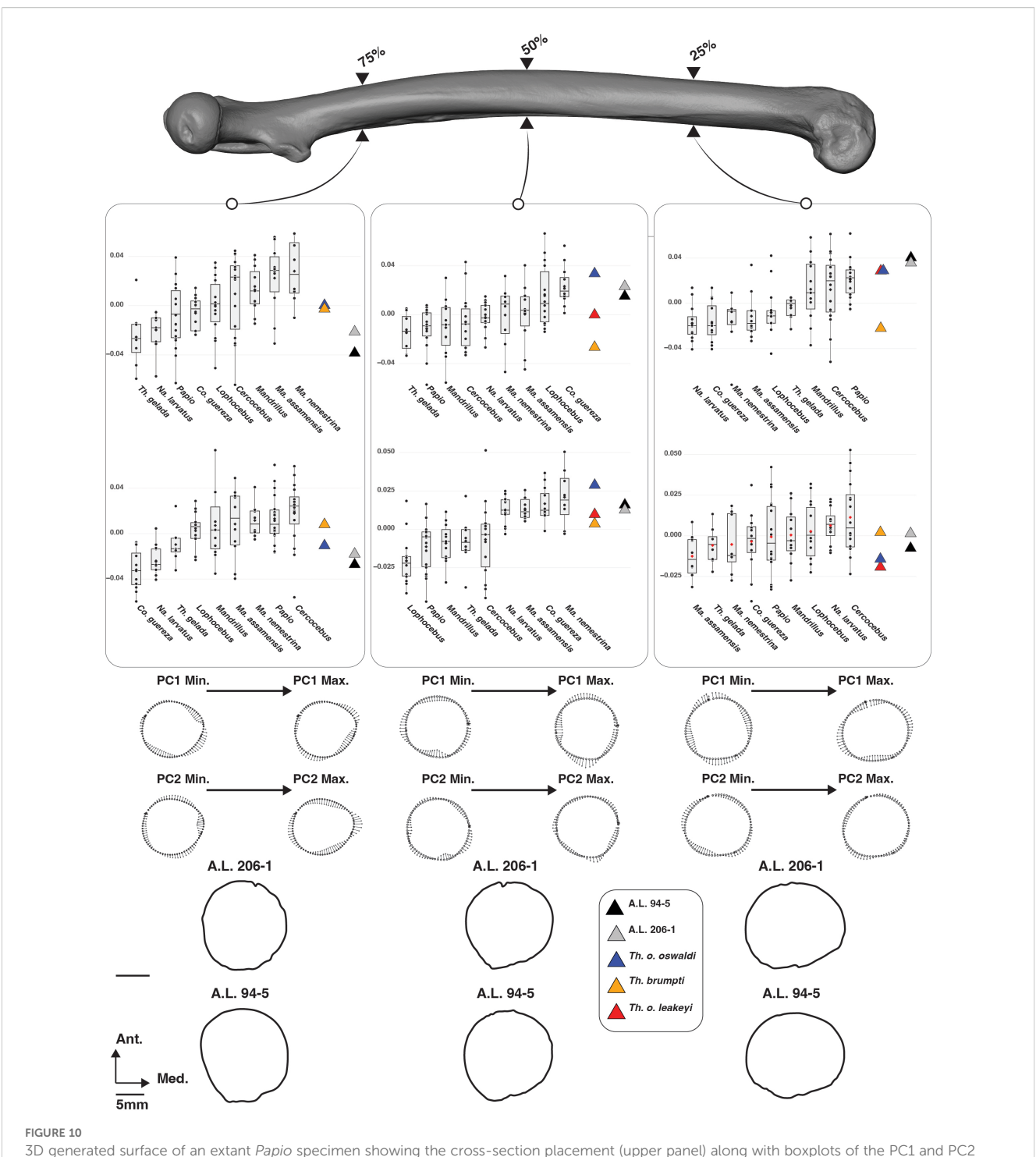
A clear clustering pattern appears on PC1 scores of the cross-sectional shape set at 25% of femoral BL. A.L. 206–1 and A.L. 94–5 show highly positive scores, matching the third quartile of *Papio*, and reflecting their mediolaterally extended distal metaphysis (Figure 10). Similar PC1 scores are observed for *T. o. oswaldi* KNM-ER 5408 and *T. o. leakeyi* Old 67-5600 but not for *T. brumpti* KNM-TH 46700 which falls on the negative side of PC1, clustering with *Macaca* and colobines. An extensive range of overlap is seen between extant taxa on PC2 scores, and all fossil *Theropithecus* show negative or slightly positive PC2 scores.

# Predictions of the LDA on complete morphometric dataset and hierarchical clustering

Although the accuracy of the linear discriminant model is modest (ca. 65%), several taxa can be classified with confidence, as is the case for *N. larvatus* (100% of correct predictions), *T. gelada* (90%), *Colobus* (75%), *Papio* (73.3%), and *Ma. assamensis* (70%). The greatest phenetic affinity of most *Theropithecus* species, as identified by posterior probability of membership, is with *T. gelada* or *Papio*, in the case of *T. o. oswaldi* KNM-ER 5408 (Figure 11A). A high phenetic affinity of A.L. 206–1 and A.L. 94–5 with *T. gelada* supports their attribution to *Theropithecus*.

Hierarchical clustering recovers a *Theropithecus* cluster with A.L. 206–1 as the sister group to extant geladas, and a *T. o. oswaldi* KNM-ER 5408 – A.L. 94–5 group sister to the *T. gelada* – A.L. 206–1 group

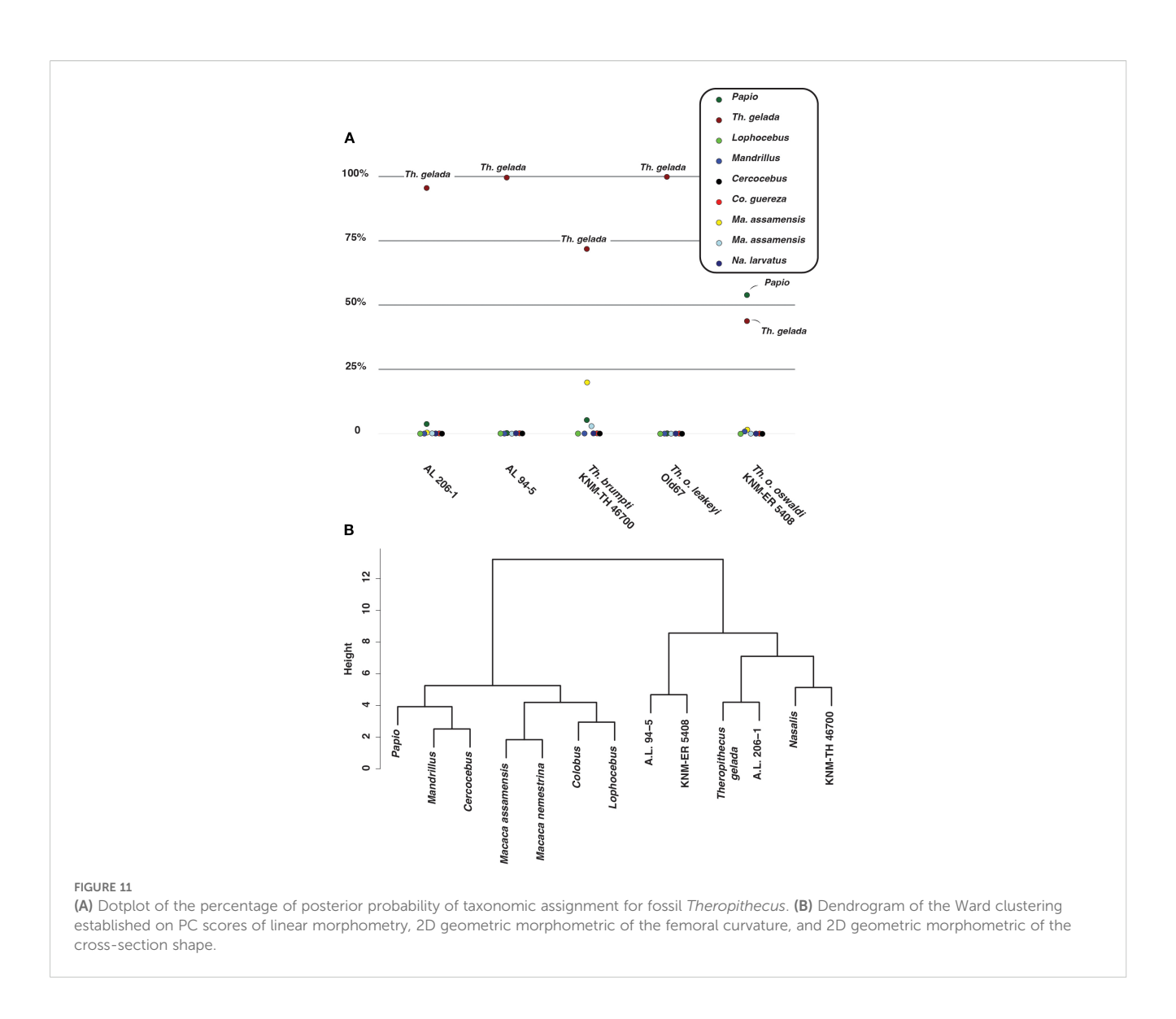
visible on the right of the boxplots



3D generated surface of an extant *Papio* specimen showing the cross-section placement (upper panel) along with boxplots of the PC1 and PC2 scores of the aligned Procrustes coordinates of the femoral cross-section outlines of extant and fossil cercopithecids (middle panel). Boxplots with median (black bar), mean (red losange), first quartile and third quartile. Shape changes along cross-section outlines on PC1 and PC2 scores are visible on the lower panel, along with the cross-section shape of A.L. 206–1 and A.L. 94–5.

(Figure 11B). Extant papionins are clustered together, to the exclusion of *Theropithecus*. The clustering of *T. brumpti* KNM-TH 46700 with *N. larvatus*, as the sister group to extant geladas and A.L. 206–1, is unexpected. Apart from a lower patellar height, a shorter femur, a more curved femur, and a more anteroposteriorly expanded diaphysis at 85% of BL, *T. brumpti* resembles *N. larvatus* for all

other considered traits included in the hierarchical analysis. The inclusion of other linear measurements (e.g., proximal projection of the greater trochanter) and qualitative traits (e.g., development of the intercondylar line) would have the potential to break down this convergence (see Supplementary Material S13 for an illustration of these traits).



# A summary of the similarities/differences in femoral anatomy between extant geladas and fossil *Theropithecus*

Overall, A.L. 206–1 shows a close phenetic match with the extant geladas, sharing 9 of the 14 considered femoral traits with them, followed by *T. brumpti*, which shares 8 of 14 femoral traits with the geladas. In contrast, *T. o. oswaldi*, with 6 out of 14 traits, and A.L. 94–5, with 4 out of 14 traits, are the least similar to geladas.

#### Discussion

We demonstrated, using a combination of LDA and hierarchical clustering established on morphometric ratios, shaft cross-sectional shape, and shaft curvature, that the subcomplete femora A.L. 206–1 (ca. 3.2 Ma) and A.L. 94–5 (ca. 2.6 Ma) exhibit closer morphological affinities with extant and fossil *Theropithecus* than with other extant papionins. Craniodental specimens of *T. o.* 

darti are documented in the Sidi Hakoma Member of the Hadar Formation, contemporaneously with A.L. 206-1 and in accordance with our taxonomic hypothesis. However, the femur A.L. 94-5 postdates the youngest T. o. darti from Hadar and slightly predates the oldest T. o. oswladi specimens from the Middle Awash, at ca. 2.5 Ma (Gamedah, Matabaietu, and Hatayae Member of the Bouri Formation; White et al., 2005 but see Getahun et al., 2023). A.L. 206-1 and A.L. 94-5 also show traits, notably on the distal femur, that distinguish them from the femur of the putative Pa. jonesi partial skeleton A.L. 363-1. It is more complicated to statistically discriminate them from Cer. meavae (A.L. 2-74), but more data are needed given the poor preservation of the femoral diaphysis of Cer. meavae. According to our phenetic analyses, age of the specimens, and current chronostratigraphic distribution of fossil *Theropithecus*, we assign A.L. 206-1 to T. cf. o. darti and A.L. 94-5 to T. cf. o. oswaldi.

No adult femora from *Theropithecus* were documented prior to the ca. 2.70 Ma *T. brumpti* femur NME L 869–1 from the Shungura Formation in the Lower Omo Valley (Pallas et al., 2023), and our

best line of evidence on the femoral anatomy of early Theropithecus relied on the ca. 3.70 Ma T. o. darti subadult partial skeleton ARI-VP-1/26 from Woranso-Mille (Frost et al., 2023). The ca. 3.20 femur A.L. 206-1 is, therefore, the earliest and most complete femoral specimen of adult Theropithecus. Similarly, no complete femora of T. o. oswaldi are known prior to 2.60 Ma, in a time where the earliest representatives of this subspecies probably emerged as suggested by craniodental data (Jablonski and Frost, 2010; Getahun et al., 2023). While A.L. 206-1 provides a unique glimpse into the mode and tempo of emergence of the adaptations of early Theropithecus, A.L. 94-5 provides new data on the functional anatomy of the earliest T. o. oswaldi. Hence, the present analysis offers new interpretations on the functional anatomy of Theropithecus postcranium and complements previous functional analyses (Krentz, 1993; Gilbert et al., 2011; Guthrie, 2011; Frost et al., 2017, 2023; Pallas et al., 2023).

### Femoral characteristics of the *T. gelada* femur

We reaffirmed, using an updated dataset from Pallas et al. (2023), that the femur of T. gelada is derived compared with that of Papio and Mandrillus by being shortened relative to body mass (Strasser, 1992), by presenting a marked asymmetry in anteroposterior depth of the condyles, and by exhibiting, relative to geometric mean, a long lever arm of the iliopsoas, an anteroposteriorly expanded femoral head, a wide intercondylar notch, a wide distal epiphysis, and a wide, shallow patellar groove (Table 3). All those adaptations are part of a functional complex that is hypothesized to be linked with squatting behaviors (Pallas et al., 2023). Indeed, the shortened femur engenders stability in crouching by lowering the center of mass, the wide femoral head enhances thigh abduction in squatted posture and the distally set lesser trochanter (i.e., an increased lever arm length of the m. iliopsoas) facilitates flexion of the thigh. The anteroposterior asymmetry of the condyles, with a deep medial one, facilitates knee abduction in flexed posture while the wide distal epiphysis and wide intercondylar notch demonstrate rotational capabilities of the knee to adjust the shank and foot position. The wide and shallow patella translates the ability to dissipate large transarticular forces generated by the m. quadriceps tendon, a major knee extensor, and a patella set preferentially in the distal position, as is the case when the knee is flexed in squatting.

# A.L. 206–1 and the emergence of squatting behaviors in *Theropithecus*

The 3.20 Ma subcomplete femur A.L. 206–1 shares with the femur of extant *T. gelada* a reduced length relative to body mass, a long lever arm length of the iliopsoas, a shallow patellar groove, a wide intercondylar notch, and a wide distal epiphysis (Table 3). On the other hand, the asymmetry of the condylar depth of A.L. 206–1 is not as marked as that of extant *T. gelada*, and its anteroposteriorly

shortened femoral head and narrow patellar groove are inconsistent with the condition seen in *T. gelada*. The total available evidence, which includes femoral curvature and femoral cross-sectional shape, demonstrates a closer phenetic affinity of A.L. 206–1 with *T. gelada*. The addition of other specimens from Hadar should demonstrate whether all traits analyzed here represent mere interindividual variation or a clear affinity between early *Theropithecus* and *T. gelada*. Unfortunately, these features are not quantified in ARI-VP 1/26, the sole published *T. o. darti* partial skeleton from eastern Africa, and its subadult status may also introduce confounding factors of ontogeny to interpret its functional anatomy.

A.L. 206-1 provides the oldest substantiated evidence for squatting behaviors in Theropithecus at ca. 3.20 Ma, with the emergence of squatting-related postcranial traits possibly as early as 3.70 Ma considering the short femur of the subadult T. o. darti subadult ARI-VP-1/26. In addition, ARI-VP-1/26 shows metacarpal proportions (i.e., elongated first metacarpal relative to the average lengths of all other metacarpals) intermediate between those of Papio and T. gelada, demonstrating that some of the postcranial traits typical of Theropithecus were not present in early members of the genus. Squatting behaviors in Theropithecus are tightly linked with grazing, with post 3 Ma fossil Theropithecus showing a derived dental and cranial anatomy related to the processing of herbaceous foods. In contrast, the earliest Theropithecus, mainly represented at Kanapoi, Woranso-Mille, Laetoli, Dikika, Makapansgat, and Hadar, among the most relevant sites, shows a less derived dental anatomy (i.e., large anterior dentition and molars with few enamel folds; Frost and Delson, 2002; Harrison, 2011; Frost et al., 2020; Getahun et al., 2023). The presence of squatting-related traits in A.L. 206-1 in a time frame where Theropithecus populations with presumed less derived dental anatomy are documented shows that the full suite characterizing the ecology of modern geladas was not in place during the mid- to late Pliocene and implies a distinct ecological niche for the earliest Theropithecus.

We attributed A.L. 206–1 to *Theropithecus* cf. oswaldi darti but the status of this subspecies in eastern Africa was recently reassessed and allocated to a new subspecies *Theropithecus oswaldi ecki*. Postcranially, there is no data that refutes this hypothesis, but given that dental and cranial arguments leading to the naming of *T. o. ecki* are mostly related to size (Eck, 1993; Getahun et al., 2023), we prefer to retain the original taxonomy of *T. o. darti* cautiously, pending a future reassessment of the cercopithecid Hadar postcranial collection.

# A.L. 94–5 and the adaptations of the earliest *Theropithecus oswaldi oswaldi*

The emergence of *Theropithecus oswaldi oswaldi* and its relationship with prior subspecies of the *Theropithecus oswaldi* species complex is in debate (Eck, 1993; Leakey, 1993; Getahun et al., 2023). The earliest *T. o. oswaldi* specimens from the Turkana Basin are now regarded as a different subspecies, either *T. o. darti* or

TABLE 3 Summary table of the main diagnostic femoral traits of T. gelada and comparison with A.L. 206-1, A.L. 94-5 and fossil Theropithecus.

	T. gelada	A.L. 206–1	A.L. 94–5	T. brumpti KNM-TH 46700	<i>T. o. oswaldi</i> KNM-ER 5408	<i>T. o. leakeyi</i> Old 67 5600
Femoral head anteroposterior expansion	Marked $\mu = 110 \pm 4.23$	Moderate 105	Moderate 106	Marked 110	Marked 112	Marked 110
Femoral neck superoinferior robustness	Moderate $\mu = 79.9 \pm 6.02$	Moderate 83.1	Marked <b>94.9</b>	Marked <b>92.1</b>	Moderate 83.3	Moderate 85.6
Femoral neck anteroposterior robustness	Marked $\mu = 66.8 \pm 5.42$	Moderate <b>60.1</b>	Extremely marked <b>75.1</b>	Marked 71.2	Marked 71.8	Marked 68.1
Relative iliopsoas lever arm length	Markedly elongated $\mu = 243 \pm 8.80$	Markedly elongated 243	Markedly elongated 233	Moderately elongated 215	Moderately elongated 222	Moderately elongated 220
Relative intercondylar notch width	Marked $\mu = 61.9 \pm 3.97$	Marked 67.4	Moderate 54.7	Marked 57.7	Moderate 48.4	Moderate 52.1
Relative biepicondylar width	Marked $\mu = 189 \pm 7.32$	Marked 187	Moderate 176	Marked 186	Moderate 175	Marked <b>193</b>
Condylar depth differential	Marked $\mu = 1.08 \pm 0.02$	Moderate 1.05	Moderate 1.04	Marked 1.09	Marked 1.10	Extremely marked 1.14
Relative patellar groove width	Marked $\mu = 98.1 \pm 3.31$	Moderate 89.5	Marked <b>96.8</b>	Moderate 87.3	Marked <b>100</b>	Moderate 87.5
Relative patellar groove height	Low $\mu = 94.7 \pm 4.33$	Low <b>91</b>	Markedly low 85.1	Low <b>92.4</b>	Markedly low <b>86.7</b>	Low <b>96.9</b>
Relative patellar groove depth	Low $\mu = 13.7 \pm 1.38$	Low 14.2	Moderate 17	Moderate 18	Moderate 17.8	Moderate 19.1
Femoral length relative to body mass	Short $\mu = -0.10 \pm 0.05$	Short <b>-0.14</b>	Short -0.13	Short -0.13	Short -0.12	Short -0.12
Femoral curvature	Moderately curved	Moderately curved	Moderately curved	Markedly curved	Poorly curved	Markedly curved
Shape of the diaphysis at 85% of BL	Markedly elliptical AP	Markedly elliptical AP	Markedly elliptical AP	Moderately elliptical AP	Moderately elliptical AP	
Shape of the diaphysis at 25% of BL	Moderately elliptical ML	Markedly elliptical AP	Markedly elliptical AP	Moderately elliptical ML	Markedly elliptical AP	

Where quantified, mean values and standard deviation are given. For fossils, traits were qualified as distinct from extant geladas and a different color cell was assigned when they fell outside the standard deviation of *T. gelada*.

Bold text indicates significant p-values.

T. o. ecki with conservative attribution to T. o. oswaldi set at ca. 2.50 Ma. With an estimated age of ca. 2.60 Ma, A.L. 94–5 is the oldest and most complete femur of T. o. oswaldi. We attributed A.L. 94–5 to T. o. oswaldi based on results of a linear discriminant analysis and a hierarchical clustering. A.L. 94–5 is more like T. cf. o. oswaldi (KNM-ER 5408) than to any other extant and fossil taxa considered. While the attribution of KNM-ER 5408 to T. o. oswaldi was not justified by Jablonski et al. (2008) on morphological grounds, the results of our morphometric analyses combined with its provenance from the Okote Member, where many T. o. oswaldi craniodental fossils were recovered, strengthen its attribution to T. o. oswaldi.

A.L. 94–5 shares with *T. gelada* a reduced length relative to body mass, a long lever arm of the iliopsoas and a wide patellar groove and marked depth differential of the condyles (Table 3). Interestingly, A.L. 94–5 bears less resemblance to *T. gelada* than A.L. 206–1, notably in lacking the wide distal epiphysis and wide intercondylar notch shared by the latter, resulting in lesser abilities

for knee rotation (Table 3). A.L. 94-5 is also distinct from T. gelada and A.L. 206-1 in its extremely robust femoral neck, a feature shared with Theropithecus brumpti and T. o. leakeyi (Gilbert et al., 2011; Pallas et al., 2023). Functionally, the robust femoral neck (superoinferiorly) of A.L. 94-5 illustrates its capacity to withstand high coronal bending loads. A.L. 94-5 and KNM-ER 5408 also show straight diaphysis that differ from those of *T. brumpti* and *T.* o. leakeyi. The functional interpretation of the femoral shaft curvature is complicated to establish given the absence of significant differences in its development between the arboreal leaper Co. guereza, the arboreal climber Ma. assamensis or the terrestrial walker and runner Papio. This feature is even more intriguing as the shaft bowing of some large Theropithecus specimens is highly distinct. Overall, the functional signal of the femur of T. o. oswaldi appears more intriguing than previously anticipated and demonstrated that even though the craniodental anatomy of this taxon is specialized for grazing, its femoral anatomy

is not fully consistent with the expected morphological pattern of a frequent squatter, notably on the distal femur, as exemplified by that of extant *T. gelada*.

Our study further demonstrates shape diversity and functional convergences in femoral anatomy among Theropithecus therefore supporting previous arguments that highlighted morphological convergences between colobines and Theropithecus in femoral head shape femoral neck robustness (Krentz, 1993). Indeed, the ressemblance of T. brumpti with Nasalis larvatus, a large colobine engaged in arboreal leaping and climbing would confirm such a convergence (Krentz, 1993; Pallas et al., 2023). This convergence is notably drawn by a robust femoral neck (anteroposteriorly and superoinferiorly). While climbing could not be ruled out to explain such similarities in shape, leaping is a much less probable candidate given the large size of T. brumpti [but see McGraw (1996) for a lack of correlation between leaping and body size for cercopithecids ranging from ca. 9-3 kg and description of female Mandrillus as adept leapers in Fleagle and McGraw (2002)]. Given the relatively gracile neck of extant T. gelada compared to T. brumpti, we expect the robust neck of T. brumpti to result from distinct selective pressures than those induced by frequent squatting behaviors or alternatively, a distinct kinetic and kinematic of squatting in the large-sized T. brumpti compared to the relatively small-sized T. gelada. Perhaps the robust neck of T. brumpti is the developmental outcome of its shortness, which also impacts the lever arm length of, among other muscles, m. vastus lateralis and the iliopsoas group. Alternatively, its short and robust neck may be the direct evidence of a yet unidentified postural/locomotor behavior requiring an extensive reinforcement of the femoral neck to bending and twisting loads. As previously suggested (Pallas et al., 2023), future kinematic and kinetic studies should investigate whether this result illustrates morphological convergences between squatters and climbers or a genuine functional signal of climbing in large Theropithecus. In addition, future quantitative analyses, including the quantification of entheses, would provide useful data to verify such functional convergences.

#### Conclusion

The femoral anatomy of fossil *Theropithecus* is poorly known prior to 2.60 Ma despite its importance in inferring the squatting posture characteristic of the grass-harvesting behavior of extant *Theropithecus gelada*. The timing of the emergence of this behavioral specificity is also debated, with dental adaptations to grazing appearing later than postcranial adaptations. At 3.2 Ma, A.L. 206–1 is the oldest known subcomplete adult femur of *Theropithecus* and provides evidence for the presence of traits related to squatting behaviors early in the evolutionary history of *Theropithecus*. We attributed A.L. 206–1 to *Theropithecus* cf. oswaldi darti and it shares with extant geladas a shortened femur, a long lever arm of the iliopsoas muscle, a wide intercondylar notch, a broad distal epiphysis, and a shallow patellar groove. At 2.60 Ma, A.L. 94–5 is the oldest and most complete femur of *Theropithecus oswaldi oswaldi* and differs from the older *T. o. darti* A.L. 206–1 by

showing a more robust neck and a less mobile distal epiphysis (narrower intercondylar notch and narrow distal epiphysis with a deeper patellar groove), further indicating diversity in femoral anatomy among fossil *Theropithecus*. We also identified phenetic affinities between *Theropithecus brumpti* and the extant leaping colobine *N. larvatus*, which underline the need to correlate skeletal traits with biomechanical data to verify functional convergences.

#### Data availability statement

The datasets presented in this study can be found in online repositories. The names of the repository/repositories and accession number(s) can be found in the article/Supplementary Material.

#### **Author contributions**

LP: Formal analysis, Writing – original draft, Project administration, Data curation, Methodology, Validation, Visualization, Resources, Software, Investigation, Supervision, Funding acquisition, Writing – review & editing, Conceptualization. MN: Validation, Investigation, Writing – review & editing, Validation. FG: Validation, Writing – review & editing, Investigation. NR: Writing – review & editing. JR: Validation, Investigation, Writing – review & editing.

#### **Funding**

The author(s) declare that no financial support was received for the research, and/or publication of this article.

#### Acknowledgments

We acknowledge the NME/EHA (Ministry of Culture and Tourism) and the NMK for granting us permission to access collections under their care and perform research. We thank the staff of the NME/EHA (T. Getachew, G. Tekle, and S. Melaku) and of the NMK (J. Kibii) for guidance and support with collections. The authors are grateful to the French Center for Ethiopian Studies (CFEE) for hosting them in Addis-Ababa while conducting research at the NME/EHA. We are also grateful to the doctoral school Theodore Monod (Faculty of Fundamental and Applied Sciences, University of Poitiers) and the Great African Rift Interdisciplinary Group of the CNRS (GDR RIFT) for financial support. The authors also wish to thank the curators and those who assisted and facilitated the acquisition of comparative data: the late W. H. Kimbel (Institute of Human Origins, Arizona State University); J. Cuisin, Museum national d'Histoire naturelle (Paris); E. Gilissen and M. Rotonda, Royal Museum for Central Africa (Tervuren), T. Nishimura, the Center for the Evolutionary Origins of Human Behavior; A. van Heteren and M. Hiermeier, the Bavarian State

Collection for Zoology. The authors would like to express their gratitude to the CFEE staff for their administrative support, and to all the field workers who participated in the field seasons that led to the discovery of the fossils from the Afar studied here.

#### Conflict of interest

The authors declare that the research was conducted in the absence of any commercial or financial relationships that could be construed as a potential conflict of interest.

#### Generative AI statement

The author(s) declare that no Generative AI was used in the creation of this manuscript.

Any alternative text (alt text) provided alongside figures in this article has been generated by Frontiers with the support of artificial

intelligence and reasonable efforts have been made to ensure accuracy, including review by the authors wherever possible. If you identify any issues, please contact us.

#### Publisher's note

All claims expressed in this article are solely those of the authors and do not necessarily represent those of their affiliated organizations, or those of the publisher, the editors and the reviewers. Any product that may be evaluated in this article, or claim that may be made by its manufacturer, is not guaranteed or endorsed by the publisher.

#### Supplementary material

The Supplementary Material for this article can be found online at: https://www.frontiersin.org/articles/10.3389/fevo.2025.1593646/full#supplementary-material

#### References

Adams, D., Collyer, M., Kaliontzopoulou, A., and Baken, E. K. (2024). *Geomorph: Software for geometric morphometric analyses. R package version 4.0.8.* Available online at: https://cran.r-project.org/package=geomorph (Accessed December 4, 2024).

Behrensmeyer, A. K. (2008). "Paleoenvironmental context of the Pliocene A.L. 333 'First Family' hominin locality, Hadar Formation, Ethiopia," in *The Geology of Early Humans in the Horn of Africa*. Eds. J. Quade and J. G. Wynn (Boulder, Colorado, USA: Geological Society of America), 203–214.

Bonnefille, R., Vincens, A., and Buchet, G. (1987). Palynology, stratigraphy and palaeoenvironment of a pliocene hominid site (2.9-3.3 M.Y.) at Hadar, Ethiopia. *Palaeogeogr. Palaeoclimatol. Palaeoecol.* 60, 249–281. doi: 10.1016/0031-0182(87)90035-6

Bouma, H. W., De Boer, S. F., De Vos, J., Van Kampen, P. M., and Hogervorst, T. (2013). Mammal hip morphology and function: coxa recta and coxa rotunda. *Anat. Rec.* 296, 250–256. doi: 10.1002/ar.22634

Campisano, C. J. (2012). Geological summary of the Busidima Formation (Plio-Pleistocene) at the Hadar paleoanthropological site, Afar Depression, Ethiopia. *J. Hum. Evol.* 62, 338–352. doi: 10.1016/j.jhevol.2011.05.002

Campisano, C. J., and Feibel, C. S. (2007). Connecting local environmental sequences to global climate patterns: evidence from the hominin-bearing Hadar Formation, Ethiopia. *J. Hum. Evol.* 53, 515–527. doi: 10.1016/j.jhevol.2007.05.015

Campisano, C. J., and Feibel, C. S. (2008). "Depositional environments and stratigraphic summary of the Pliocene Hadar Formation at Hadar, Afar Depression, Ethiopia," in *The Geology of Early Humans in the Horn of Africa*. Eds. J. Quade and J. G. Wynn (Boulder, Colorado, USA: Geological Society of America), 179–201.

Campisano, C. J., Rowan, J., and Reed, K. E. (2022). "The hadar formation, afar regional state, Ethiopia: geology, fauna, and paleoenvironmental reconstructions," in *African Paleoecology and Human Evolution*. Eds. S. C. Reynolds and R. Bobe (Cambridge, UK: Cambridge University Press), 214–228. doi: 10.1017/9781139696470.018

Cignoni, P., Callieri, M., Corsini, M., Dellepiane, M., Ganovelli, F., and Ranzuglia, G. (2008). "MeshLab: an open-source mesh processing tool," in *Eurographics Italian Chapter Conference*, Vol. 8. doi: 10.2312/LOCALCHAPTEREVENTS/ITALCHAP/ITALIANCHAPCONF2008/129-136

Cooke, S. B., and Tallman, M. (2012). New endemic platyrrhine femur from Haiti: Description and locomotor analysis. *J. Hum. Evol.* 63, 560–567. doi: 10.1016/j.jhevol.2012.05.008

Delson, E., Eck, G. G., Leakey, M. G., and Jablonski, N. G. (1993). "Appendix I A partial catalogue of fossil remains of *Theropithecus*," in Theropithecus: *The rise and fall of a primate genus*. Ed. N. G. Jablonski (Cambridge University Press, Cambridge), 499–526.

DeSilva, J. M., McNutt, E., Zipfel, B., Ward, C. V., and Kimbel, W. H. (2020). Associated *Australopithecus afarensis* second and third metatarsals (A.L. 333-133) from Hadar, Ethiopia. *J. Hum. Evol.* 146, 102848. doi: 10.1016/j.jhevol.2020.102848

DiMaggio, E. N., Campisano, C. J., Rowan, J., Dupont-Nivet, G., Deino, A. L., Bibi, F., et al. (2015). Late Pliocene fossiliferous sedimentary record and the environmental context of early *Homo* from Afar, Ethiopia. *Science* 347, 1355–1359. doi: 10.1126/science.aaa1415

Drapeau, M. S. M., Ward, C. V., Kimbel, W. H., Johanson, D. C., and Rak, Y. (2005). Associated cranial and forelimb remains attributed to *Australopithecus afarensis* from Hadar, Ethiopia. *J. Hum. Evol.* 48, 593–642. doi: 10.1016/j.jhevol.2005.02.005

Eck, G. G. (1993). "Theropithecus darti from the hadar formation, Ethiopia," in Theropithecus: The rise and fall of a primate genus. Ed. N. G. Jablonski (Cambridge University Press, Cambridge), 15–76.

Fleagle, J. G., and McGraw, W. S. (2002). Skeletal and dental morphology of African papionins: unmasking a cryptic clade. *J. Hum. Evol.* 42, 267–292. doi: 10.1006/jhev.2001.0526

Fleagle, J. G., and Meldrum, J. D. (1988). Locomotor behaviors and skeletal morphology of two sympatric pitheciine monkeys, *Pithecia pithecia* and *Chiropotes satanas*. *Am. J. Primatol.* 16, 227–249. doi: 10.1002/ajp.1350160305

Fleagle, J. G., and Simons, E. L. (1995). Limb skeleton and locomotor adaptations of apidium phiomense an oligocene anthropoid from Egypt. Am. J. Phys. Anthropol. 97, 235–289. doi: 10.1002/ajpa.1330970303

Ford, S. M. (1988). Postcranial adaptations of the earliest platyrrhine. *J. Hum. Evol.* 17, 155–192. doi: 10.1016/0047-2484(88)90053-X

Frost, S. R., and Delson, E. (2002). Fossil Cercopithecidae from the Hadar Formation and surrounding areas of the Afar Depression, Ethiopia. *J. Hum. Evol.* 43, 687–748. doi: 10.1006/jhev.2002.0603

Frost, S. R., Jablonski, N. G., and Haile-Selassie, Y. (2023). The earliest most complete skeleton of *Theropithecus. J. Hum. Evol.* 180, 103370. doi: 10.1016/j.jhevol.2023.103370

Frost, S. R., Saanane, C., Starkovich, B. M., Schwartz, H., Schrenk, F., and Harvati, K. (2017). New cranium of the large cercopithecid primate *Theropithecus oswaldi leakeyi* (Hopwood 1934) from the paleoanthropological site of Makuyuni, Tanzania. *J. Hum. Evol.* 109, 46–56. doi: 10.1016/j.jhevol.2017.05.007

Frost, S. R., Ward, C. V., Manthi, F. K., and Plavcan, J. M. (2020). Cercopithecid fossils from kanapoi, West Turkana, Kenya, (2007–2015). *J. Hum. Evol.* 140, 102642. doi: 10.1016/j.jhevol.2019.102642

Gebo, D. L., and Sargis, E. J. (1994). Terrestrial adaptations in the postcranial skeletons of guenons. *Am. J. Phys. Anthropol.* 93, 341–371. doi: 10.1002/ajpa.1330930306

Getahun, D. A., Delson, E., and Seyoum, C. M. (2023). A review of *Theropithecus oswaldi* with the proposal of a new subspecies. *J. Hum. Evol.* 180, 103373. doi: 10.1016/j.jhevol.2023.103373

Gilbert, C. C., Goble, E. D., Kingston, J. D., and Hill, A. (2011). Partial skeleton of *Theropithecus brumpti* (Primates, Cercopithecidae) from the Chemeron Formation of the Tugen Hills, Kenya. *J. Hum. Evol.* 61, 347–362. doi: 10.1016/j.jhevol.2011.04.007

Groves, C. P., and Butynski, T. M. (2016). "Genus lophocebus baboon-mangabeys (Grey-cheeked mangabeys, black mangabeys)," in *Mammals of Africa Volume II Primates*. Eds. T. Butynski, J. Kingdon and J. Kalina (Bloomsbury Publishing, London), 204–205.

Guthrie, E. H. (2011). Functional morphology of the postcranium of *Theropithecus brumpti* (Primates: Cercopithecidae). [dissertation thesis]. University of Oregon, Oregon (Or).

Harrison, T. H. (2011). "Cercopithecids (Cercopithecidae, primates)," in Paleontology and geology of Laetoli: Human evolution in context. Fossil hominins and the associated fauna. Ed. T. Harrison (Springer, Dordrecht), 83–140.

Hirasaki, E., Malaivijitnond, S., and Hamada, Y. (2019). Locomotor kinematics of two semi-wild macaque species (*Macaca assamensis* and *Macaca arctoides*) in Thailand. Fol. Primatol. 90, 162–178. doi: 10.1159/000496024

Iwamoto, T. (1993). "The ecology of *Theropithecus gelada*," in Theropithecus: *The rise and fall of a primate genus*. Ed. N. G. Jablonski (Cambridge University Press, Cambridge), 441–452.

Jablonski, N. J., and Frost, S. R. (2010). "Cercopithecoidea," in *Cenozoic Mammals of Africa*. Eds. L. Werdelin and J. W. Sanders (University of California Press, Oakland, CA), 393–428.

Jablonski, N. G., Leakey, M. G., and Anton, M. (2008). "Systematic paleontology of the cercopithecines," in *Koobi Fora Research Project, Volume 6: The Fossil Monkeys*. Eds. N. G. Jablonski and M. G. Leakey (California Academy of Sciences, San Francisco, CA) 103-300

Johanson, D. C., Lovejoy, C. O., Kimbel, W. H., White, T. D., Ward, S. C., Bush, M. E., et al. (1982a). Morphology of the Pliocene partial hominid skeleton (A.L. 288-1) from the Hadar formation, Ethiopia. *Am. J. Phys. Anthropol.* 57, 403–451. doi: 10.1002/ajpa.1330570403

Johanson, D. C., Taieb, M., and Coppens, Y. (1982b). Pliocene hominids from the Hadar formation, Ethiopia (1973–1977): Stratigraphic, chronologic, and paleoenvironmental contexts, with notes on hominid morphology and systematics. *Am. J. Phys. Anthropol.* 57, 373–402. doi: 10.1002/ajpa.1330570402

Jolly, C. J. (2016a). "Genus papio baboons," in Mammals of Africa Volume II Primates. Eds. T. Butynski, J. Kingdon and J. Kalina (Bloomsbury Publishing, London), 217–218.

Jolly, C. J. (2016b). "Genus theropithecus gelada," in Mammals of Africa Volume II Primates. Eds. T. Butynski, J. Kingdon and J. Kalina (Bloomsbury Publishing, London), 239.

Kimbel, W. H., and Delezene, L. K. (2009). Lucy" redux: A review of research on Australopithecus afarensis. Am. J. Phys. Anthropol. 140, 2-48. doi: 10.1002/ajpa.21183

Kimbel, W. H., Johanson, D. C., and Rak, Y. (1994). The first skull and other new discoveries of *Australopithecus afarensis* at Hadar, Ethiopia. *Nature* 368, 449–451. doi: 10.1038/368449a0

Kimbel, W. H., Walter, R. C., Johanson, D. C., Reed, K. E., Aronson, J. L., Assefa, Z., et al. (1996). Late pliocene homo and oldowan tools from the hadar formation (Kada hadar member), Ethiopia. *J. Hum. Evol.* 31, 549–561. doi: 10.1006/jhev.1996.0079

Kingdon, J., and Groves, C. P. (2016a). "Genus *cercocebus* drill-mangabeys (White-eyelid mangabeys)," in *Mammals of Africa Volume II Primates*. Eds. T. Butynski, J. Kingdon and J. Kalina (Bloomsbury Publishing, London), 165–167.

Kingdon, J., and Groves, C. P. (2016b). "Genus colobus black-and-white colobus monkeys," in *Mammals of Africa Volume II Primates*. Eds. T. Butynski, J. Kingdon and J. Kalina (Bloomsbury Publishing, London), 95–96.

Krentz, H. B. (1993). "Postcranial anatomy of extant and extinct species of *Theropithecus*," in Theropithecus: *The rise and fall of a primate genus*. Ed. N. G. Jablonski (Cambridge University Press, Cambridge), 383–425.

Kuhn, M. (2008). Building predictive models in R using the caret package. J. Stat. Soft. 28, 1–26. doi: 10.18637/jss.v028.i05

Latimer, B., Ohman, J. C., and Lovejoy, O. C. (1987). Talocrural joint in african hominoids: implications for *australopithecus afarensis*. *Am. J. Phys. Anthropol.* 74, 155–175. doi: 10.1002/ajpa.1330740204

Leakey, M. G. (1993). "Evolution of *theropithecus* in the turkana basin," in Theropithecus: *The rise and fall of a primate genus*. Ed. N. G. Jablonski (Cambridge University Press, Cambridge), 85–124.

Lepre, C. J., and Kent, D. V. (2015). Chronostratigraphy of KNM-ER 3733 and other Area 104 hominins from Koobi Fora. J. Hum. Evol. 86, 99–111. doi: 10.1016/j.jhevol.2015.06.010

Lifshitz, L., Bar Sela, S., Gal, N., Martin, R., and Fleitman Klar, M. (2020). Iliopsoas the hidden muscle: anatomy, diagnosis, and treatment. *Curr. Sports Med. Rep.* 19, 235–243. doi: 10.1249/JSR.00000000000000723

Madar, S. I., Rose, M. D., Kelley, J., MacLatchy, L., and Pilbeam, D. (2002). New *Sivapithecus* postcranial specimens from the Siwaliks of Pakistan. *J. Hum. Evol.* 42, 705–752. doi: 10.1006/jhev.2002.0554

McGraw, S. W. (1996). Cercopithecid locomotion, support use, and support availability in the Tai Forest, Ivory Coast. *Am. J. Phys. Anthropol.* 100, 507–522. doi: 10.1002/(SICI)1096-8644(199608)100:4<507::AID-AJPA5>3.0.CO;2-N

Mosimann, J. E. (1970). Size allometry: size and shape variables with characterizations of the lognormal and generalized gamma distributions. *J. Am. Stat. Assoc.* 65, 930–945. doi: 10.1080/01621459.1970.10481136

Murtagh, F., and Legendre, P. (2014). Ward's hierarchical agglomerative clustering method: which algorithms implement ward's criterion? *J. Classif.* 31, 274–295. doi: 10.1007/s00357-014-9161-z

Nakatsukasa, M. (1994). Morphology of the humerus and femur in African mangabeys and guenons: functional adaptation and implications for the evolution of positional behavior. *Afr. Stud. Monogr.* 21, 1–61. doi: 10.14989/68371

Ogle, D., Doll, J., Wheeler, A., and Dinno, A. (2023). FSA: Simple Fisheries Stock Assessment Methods. *R package version 0.9.4*. CRAN. doi: 10.32614/CRAN.package.FSA

Oksanen, J., Simpson, G. L., Blanchet, F. G., Kindt, R., Legendre, P., Minchin, P. R., et al. (2001). vegan: Community Ecology Package. 2.6-8. doi: 10.32614/CRAN.package.vegan

Pallas, L., Daver, G., Merceron, G., and Boisserie, J.-R. (2023). The anatomy of the hindlimb of *Theropithecus brumpti* (Cercopithecidae, Papionini): Morphofunctional implications. *J. Hum. Evol.* 178, 103333. doi: 10.1016/j.jhevol.2023.103333

Radosevich, S. C., Retallack, G. J., and Taieb, M. (1992). Reassessment of the paleoenvironment and preservation of hominid fossils from Hadar, Ethiopia. *Am. J. Phys. Anthropol.* 87, 15–27. doi: 10.1002/ajpa.1330870103

R Core Team (2024). R: A language and environment for statistical computing. Available online at: https://www.R-project.org/.

Rector, A. L., and Vergamini, M. (2018). Forelimb morphology and substrate use in extant Cercopithecidae and the fossil primate community of the Hadar sequence, Ethiopia. *J. Hum. Evol.* 123, 70–83. doi: 10.1016/j.jhevol.2018.06.005

Reed, K. E. (2008). Paleoecological patterns at the Hadar hominin site, Afar Regional State, Ethiopia. J. *Hum. Evol.* 54, 743–768. doi: 10.1016/j.jhevol.2007.08.013

Rodman, P. S. (1979). Skeletal differentiation of *Macaca fascicularis* and *Macaca nemestrina* in relation to arboreal and terrestrial quadrupedalism. *Am. J. Phys. Anthropol.* 51, 51–62. doi: 10.1002/ajpa.1330510107

Rohlf, F. J. (2006). *tpsDig, Digitize Landmarks and Outlines*. State University of New York at Stony Brook: New York: Department of Ecology and Evolution.

Rowan, J., Lazagabaster, I. A., Campisano, C. J., Bibi, F., Bobe, R., Boisserie, J.-R., et al. (2022). Early Pleistocene large mammals from Maka'amitalu, Hadar, lower Awash Valley, Ethiopia. *PeerJ* 10, e13210. doi: 10.7717/peerj.13210

Ruff, C. B. (2003). Long bone articular and diaphyseal structure in Old World monkeys and apes. II: Estimation of body mass. *Am. J. Phys. Anthropol.* 120, 16–37. doi: 10.1002/ajpa.10118

Stanistreet, I. G. (2012). Fine resolution of early hominin time, Beds I and II, Olduvai Gorge, Tanzania. *J. Hum. Evol.* 63, 300–308. doi: 10.1016/j.jhevol.2012.03.001

Strasser, E. (1992). Hindlimb proportions, allometry, and biomechanics in old world monkeys (Primates, cercopithecidae). *Am. J. Phys. Anthropol.* 87, 187–213. doi: 10.1002/ajpa.1330870207

Susman, R. L., Stern, J. T., and Jungers, W. L. (1984). Arboreality and bipedality in the hadar hominids. *Folia Primatol.* 43, 113–156. doi: 10.1159/000156176

Szalay, F. S., and Delson, E. (1979). "Evolutionary history of the primates," (Academic Press, New York).

Tardieu, C. (1983). L'articulation du genou des primates catarhiniens et hominides fossiles. Implications phylogenetique et taxinomique. *BMSAP* 10, 355–372. doi: 10.3406/bmsap.1983.3908

Venables, W. N., and Ripley, B. D. (1997). Modern Applied Statistics with S-PLUS (New York, NY: Springer New York). doi: 10.1007/978-1-4757-2719-7

Villmoare, B., Kimbel, W. H., Seyoum, C., Campisano, C. J., DiMaggio, E. N., Rowan, J., et al. (2015). Early homo at 2.8 ma from ledi-geraru, afar, Ethiopia. *Science* 347, 1352–1355. doi: 10.1126/science.aaa1343

Ward, C. V. (1993). Partial skeleton of *proconsul nyanzae* from mfangano island, Kenya. *Am. J. Phys. Anthropol.* 90, 77–111. doi: 10.1002/ajpa.1330900106

Ward, C. V., Kimbel, W. H., Harmon, E. H., and Johanson, D. C. (2012). New postcranial fossils of *Australopithecus afarensis* from Hadar, Ethiopia (1990–2007). *J. Hum. Evol.* 63, 1–51. doi: 10.1016/j.jhevol.2011.11.012

White, T. D., Asfaw, B., and Suwa, G. (2005). Pliocene hominid fossils from Gamedah, Middle Awash, Ethiopia. *Trans. R. Soc S. Afr.* 60, 79–83. doi: 10.1080/00359190509520481

White, T. D., and Johanson, D. C. (1982). Pliocene hominid mandibles from the Hadar formation, Ethiopia: 1974-1977 collections. *Am. J. Phys. Anthropol.* 57, 501–544. doi: 10.1002/ajpa.1330570405